

THESIS

DECREASED DICAMBA TRANSPORT DUE TO INCREASED FLAVONOID
BIOSYNTHESIS: A CANDIDATE DICAMBA RESISTANCE MECHANISM

Submitted by

Dean J. Pettinga

Department of Bioagricultural Sciences and Pest Management

In partial fulfillment of the requirements

For the Degree of Master of Science

Colorado State University

Fort Collins, Colorado

Fall 2016

Master's Committee

Advisor: Todd A. Gaines

Sarah Ward
Daniel Sloan

Copyright by Dean Jacob Pettinga 2016

All Rights Reserved

ABSTRACT

DECREASED DICAMBA TRANSPORT DUE TO INCREASED FLAVONOID BIOSYNTHESIS: A CANDIDATE DICAMBA RESISTANCE MECHANISM

Resistance to dicamba (a synthetic auxin herbicide) has been documented in *Kochia scoparia* (L.) Schrad. populations since 1994, but the molecular mechanisms of observed resistance cases remain elusive. An RNA-Seq approach was used to identify transcripts with significantly differential transcription responses between inbred lines of dicamba-resistant (9425R) and dicamba-susceptible (7710S) *K. scoparia* in response to dicamba application. Among the significantly differentially expressed transcripts was both Chalcone Synthase (CHS), the first enzyme and rate-limiting step in the flavonoid biosynthesis pathway, and Flavonol 3'-Hydroxylase (F3'H), which catalyzes the conversion of quercetin into kaempferol, known inhibitors of auxin transport. *In silico* expression patterns of both transcripts were confirmed with qRT-PCR. An F₂ population derived from a cross of 9425R x 7710S segregating for the resistance phenotype was assayed for CHS and F3'H expression using qRT-PCR. Dicamba-resistant F₂ individuals displayed significantly higher CHS transcript abundance compared to dicamba-susceptible F₂ individuals, associating the resistance phenotype of 9425R with a greater overall flux through the flavonoid biosynthesis pathway. Increased production of the auxin transport inhibitors quercetin and kaempferol could reduce intercellular transport and vascular loading of dicamba, causing a substantial reduction in dicamba efficacy by reducing its translocation to sensitive meristematic tissue, thereby conferring the observed resistance phenotype.

ACKNOWLEDGEMENTS

Illumina sequencing was performed at the University of Illinois Roy J. Carver Biotechnology Center (CBC) High-Throughput Sequencing and Genotyping Unit. Funding for this research was provided by BASF Corporation.

DEDICATION

This thesis is dedicated to my parents, Ross and Jonell Pettinga. Their encouragement and support has enabled my passion for science and pursuit of lifelong learning.

TABLE OF CONTENTS

Abstract	ii
Acknowledgements	iii
Dedication	iv
List of Tables	vii
List of Figures	viii
Chapter 1: <i>Kochia scoparia</i> , Auxin, and Dicamba	1
<i>Kochia scoparia</i>	1
Overview	1
Agronomic Success	2
Abiotic Tolerance	2
Herbicide Resistance	3
Auxin Biology: <i>Arabidopsis thaliana</i>	5
Auxin Perception	5
Auxin Transport	6
Dicamba Herbicide	8
Overview and Mode of Action	8
Dicamba Resistance	9
Chapter 2: Understanding Dicamba Resistance in <i>Kochia scoparia</i> – a Functional Genomics Approach	13
Introduction	13
Methods	14
Characterization of Lines	14
Dicamba Dose Response	14
Statistical Analysis	14
RNA-Seq	15
Plant Material	15
Alignment and Differential Expression	16
SNP Genotyping from RNA-Seq Alignments	18
Validation of <i>in silico</i> Candidate Expression via qRT-PCR	19
Hypothesis Testing: Forward Genetics	20
Breeding	21
Relative Expression Quantification	21
CHS Copy Number Quantification	22
Results	22
Characterization of Lines: Dicamba Dose Response	22
RNA-Seq:	23
Differential Expression	23
Auxin Receptor and Transporter SNPs	24
Hypothesis Generation	24
Hypothesis Validation	26
qRT-PCR Validation of Candidate <i>in silico</i> Expression	26
Forward Genetics: Candidate Expression and CHS Copy Number	28

Discussion	29
RNA-Seq: Conclusions	29
Further Work: Mutant Analysis, Analytical Chemistry, and Mapping	30
References	50
Appendix: TWD1 Genotyping	56
Introduction	56
Role of TWD1 in Auxin Transport	56
Methods	56
TWD1 Genotyping	56
S262G KASP Assay	57
Results and Discussion	58

LIST OF TABLES

Table 1 – Real-Time PCR Primers	33
Table 2 – Dose Response Curve Variables	34
Table 3 – SNP Calls and Differential Expression: Auxin Receptors and Transporters.....	35
Table 4 – F ₂ Phenotypic Distribution.....	36
Table 5 – TWD1 KASP Genotyping Primers.....	59

LIST OF FIGURES

Figure 1 – Dicamba Dose Response Curves.....	37
Figure 2 – Dicamba Dose Response Image	38
Figure 3 – RNA-seq Principle Components Analysis	39
Figure 4 – GLM Terms: Venn Diagram	40
Figure 5 – Line*Treatment GeneCloud	41
Figure 6 – Line*Treatment Heatmap	42
Figure 7 – Flavonol Biosynthesis Pathway in <i>Arabidopsis thaliana</i>	43
Figure 8 – Flavonol Biosynthesis: <i>in silico</i> Expression	44
Figure 9 – ABCB Auxin Transporters: <i>in silico</i> Expression	45
Figure 10 – qRT-PCR and <i>in silico</i> Expression Regression	46
Figure 11 – qRT-PCR Validation of Flavonol Biosynthesis Expression	47
Figure 12 – CHS Genomic Copy Number	48
Figure 13 – Co-segregation of Flavonol Biosynthesis Expression Profile with Phenotype in F ₂ ..	49
Figure 14 – TWD1 cDNA Alignment	60
Figure 15 – TWD1 Protein Alignment	61
Figure 16 – TWD1 F ₂ Genotyping	62

KOCHIA SCOPARIA

Overview

Kochia scoparia is an annual, herbaceous plant native to Eurasia. It was likely introduced to North America as an ornamental where it subsequently escaped cultivation, forming wild populations (Friesen et al., 2009). Since its escape from cultivation, this species has become one of the most problematic weedy species for cereal, soybean, and sugar beet production in the western high plains of North America (Bell et al., 1972; Mengitsu and Messersmith, 2002). A monoecious species, *K. scoparia* produces protogynous flowers wherein stigma emerge and are receptive to pollen before the anthers within the same flower release pollen. In addition, its shoot architecture mediates the above-ground biomass to break off at an abscission layer formed at the base during senescence and disperse seed in a tumbling fashion (Friesen et al., 2009). This method of seed dispersal has proven highly effective. Reports have identified individuals dispersing up to approx. 100,000 seeds up to 1 km (Beckie et al., 2016). The high rates of outcrossing mediated by the flowering system and long-distance seed dispersal through tumbling contribute to the high rates of gene flow observed within and among *K. scoparia* populations (Mengitsu and Messersmith, 2002; Friesen et al., 2009). In accordance, the species displays immense morphological diversity. The high genetic diversity has enabled adaptation to many selection pressures making the species successful in agronomic systems.

Agronomic Success

K. scoparia has successfully invaded no tillage (no-till) agronomic systems common to the western high plains of North America. Reports have shown up to twice the abundance of *K. scoparia* populations in no-till systems compared to conventional tillage systems (Friesen et al., 2009). This relative abundance may be explained both due to *K. scoparia*'s ability to germinate and establish early in the growing season when crop residues maintain cool soil temperatures (Friesen et al., 2009), leading to rates of soil seedbank recruitment up to four times higher than in conventional tillage systems. In addition, reduced tillage and dependence on chemical management strategies increases selection pressure for herbicide resistant phenotypes, which can rapidly dominate populations.

Abiotic Tolerance

K. scoparia's tolerances to abiotic stress have greatly contributed to its success as an invasive species of croplands. Its tolerance to salt stress may be partially explained by its requirement for sodium as a micronutrient due to utilizing NADP-ME in C₄ photosynthesis (Pyankov et al., 1999). In addition to its specific requirement for sodium, *K. scoparia*'s C₄ photosynthesis also likely contributes to its high water use efficiency and therefore drought tolerance. The high photosynthetic output to transpiration ratio associated with this type of photosynthesis greatly contributes to its high water use efficiency (Wiese and Vandiver, 1970; Nussbaum et al., 1985; Collins and Jones, 1986). In addition to physiological advantages for water use efficiency, *K. scoparia*'s morphology is partially responsible for drought tolerance, with roots extending down to depths of 5m (Friesen et al., 2009). Finally, *K. scoparia* displays remarkable cold tolerance. It is able to germinate and emerge as early as March, with later

flushes possible throughout the growing season as moisture becomes available (Evetts and Burnside, 1972; Schwingamer and Van Acker, 2008). Upon germination, emerged seedlings display tolerance to frost, enabling successful early establishment. The early establishment allows it to outcompete other weeds and crops, while continuous germination allows for temporal avoidance of management strategies such as tillage and herbicide application.

Herbicide Resistance

In response to the intense selection pressure generated by herbicide application, *K. scoparia* has evolved numerous resistance phenotypes. Its ability to rapidly evolve resistant populations has further contributed to its success in cropping systems. The first documented cases of herbicide-resistant *K. scoparia* were atrazine-resistant populations found in Kansas during the late 1970s (Heap, 2016). To date, fifty-four unique *K. scoparia* populations worldwide have evolved resistance to twenty-four unique herbicide molecules, comprising four herbicidal modes of action including photosystem II inhibition, Acetolactate Synthase inhibition (branched-chain amino acid biosynthesis), EPSP Synthase inhibition (aromatic amino acid biosynthesis), and synthetic auxins (Heap, 2016). Resistance to auxinic herbicides 2,4-Dichlorophenoxyacetic acid (2,4-D) and dicamba are of particular current interest. Transgenic crops engineered for tolerance to each of these herbicides are expected to be approved for planting and post-emergence application of dicamba or 2,4-D (Behrens et al., 2007; Wright et al., 2010; Cao et al., 2011). Glyphosate-tolerant cropping systems were one of the most rapidly adopted weed management technologies in history following their introduction in 1996 (Dill et al., 2008). Glyphosate-resistant weed populations were first reported in 1998 (Powles et al., 1998), nearly 30 years after the introduction of glyphosate as a herbicide. Glyphosate-resistant

weed populations emerged as a major agricultural threat in agronomic crops due to the intense selection pressure generated by use of glyphosate in glyphosate-resistant crops without additional diversity in control methods (Powles, 2008). Research on current cases of dicamba and 2,4-D herbicide-resistant weedy populations before the release of the respective tolerant cropping systems presents an opportunity to predict the inheritance and mechanisms of inevitable future resistance cases before they evolve under intense selection pressure. This research provides insights for management and prevention of herbicide-resistance evolution in these next-generation cropping technology systems.

Since 1994, there have been eight documented cases of dicamba-resistant *K. scoparia* populations located throughout the western high plains of North America (Heap, 2016). Studies have failed to identify differences in dicamba uptake, translocation, or metabolism between resistant and susceptible biotypes (Cranston et al., 2001), but differences in root growth inhibition and gravitropism suggest that resistance in some populations may result from mutations in auxin signaling pathways (Goss and Dyer, 2003). Gene expression analysis of resistant and susceptible lines identified differences in expression of ACC synthase and a putative chloride transporter (Kern et al., 2005), but no validation experiments have confirmed the necessity of the observed transcription patterns for the corresponding resistant and susceptible phenotypes. To date, research on various dicamba-resistant *K. scoparia* populations has concluded that the observed phenotypes are likely results of differential perception of dicamba due to mutated auxin receptors or auxin-signaling genes (Cranston et al., 2001; Goss and Dyer, 2003), but no conclusive evidence has yet linked a molecular mechanism to any dicamba-resistance phenotype.

AUXIN BIOLOGY: *ARABIDOPSIS THALIANA*

Auxin Perception

Modern understanding of auxinic herbicide mode of action is derived from the vast body of research on the perception and signaling of indole-3-acetic acid (IAA) using the intensively studied model plant, *Arabidopsis thaliana*. This body of research has identified three core auxin signaling pathways initiated by the following receptor systems: Auxin Binding Protein 1-Transmembrane Kinase (ABP1-TMK) (Xu et al., 2014), S-Phase Kinase-Associated Protein 2A (SKP2A) (Jurado et al., 2010), and the SCF^{TIR1/AFBs} complex [SKP-Cullin F-Box (SCF), TRANSPORT INHIBITOR RESISTANT 1/ AUXIN-SIGNALING F-BOX (TIR1/AFB)] (Salehin et al., 2015). Receptors transduce the auxin signal through both unique and overlapping pathways involving a complex series of protein degradations, de-repressions, and transcriptional upregulation, resulting in rapid changes in cell morphology, polarization, elongation, division, and differentiation (Sauer et al., 2013).

Since its discovery nearly 40 years ago, Auxin Binding Protein 1 (ABP1) has been proposed as an auxin receptor. This protein is located in the apoplast, and associates with Transmembrane Kinases (TMKs) that transduce the auxin signal into the cytoplasm by activating ROPs [Rho-like guanosine triphosphatases (GTPases)] also associated with the cell membrane (Wu et al., 2011; Xu et al., 2014; Grones et al., 2015). This activation of ROPs leads to cytoskeletal rearrangements and regulates cell expansion (Rodriguez-Serrano et al., 2014). Additionally, ROP activity induces clathrin-dependent endocytosis of PIN-FORMED (PIN) auxin transporters (Robert et al., 2010), inducing changes in auxin concentration gradients among the root meristem and surrounding tissues. These activities produce changes in cell growth and differentiation, two important effects of auxin.

Transport Inhibitor Resistant 1 (TIR1) and Auxin Signaling F-Box proteins (AFBs) are F-box proteins which interact with a cullin (CUL1) and SKP1-like proteins (ASK1 or ASK2) to form SCF ubiquitin ligase complexes (Gray et al., 2001). This complex perceives auxin in conjunction with Aux/IAA transcriptional repressors, which recruit 26S proteasomes to degrade the Aux/IAs, thus releasing Auxin Response Factor (ARFs) transcription factors from repression (Gray et al., 2001). Through the activity of de-repressed ARFs, a number of diverse developmental processes are promoted including cellular elongation, differentiation, and division.

The recently discovered auxin receptor, SKP2A is an F-box protein which acts as a positive regulator of auxin response and cellular division (Jurado et al., 2010). Root growth experiments using *A. thaliana* with mutations in both TIR1 and SKP2A showed an additive effect on auxin-resistant growth, implicating SKP2A activity in auxin response (Jurado et al., 2010). Further, SKP2A promotes division by targeting E2FC and DPB, known transcriptional repressors of cell-division (del Pozo et al., 2006). This function aligns with SKP2A's regulation of auxin response through auxin perception with a binding pocket analogous to that observed in SCF^{TIR1/AFB} complexes (Jurado et al., 2010).

Auxin Transport

The effects of auxin are dependent upon concentrations and gradients. Local gradients are important not only for determining the direction of auxin-induced growth, but also tissue differentiation and development (Sabatini et al., 1999; Benková et al., 2003; Blilou et al., 2005; Grieneisen et al., 2007). In addition to IAA diffusion across biological membranes according to the chemiosmotic model (Goldsmith, 1977), several families of auxin transporters (PINs,

AUX/LAX, ABC Transporters) control the flow of auxin across subcellular compartments and the cell membrane. In many cases, not only are expression and regulation of their transport activity important, but their location on the cellular membrane plays an important role in distributing auxin to other cells, establishing the required concentration gradients necessary for coordinated growth and differentiation among cells for proper development.

Polar auxin transport (PAT), wherein transporters exhibit asymmetric localization in the plasma membrane and direct intercellular auxin flow is controlled by the membrane-bound efflux proteins of the PIN-FORMED (PINs) and influx proteins in the AUX/LAX family (Kleine-Vehn et al., 2010; Swarup and Péret, 2012). The eight members of the *A. thaliana* PIN family have different localizations within the plasma membrane or on the ER with specific directional auxin efflux and cellular homeostasis associated with each protein (Gälweiler et al., 1998; Friml et al., 2002; Blilou et al., 2005; Zazimalova et al., 2010; Simon et al., 2016). In conjunction, the four *A. thaliana* AUX/LAX members serve as influx transporters for PAT. Developmentally, this gene family regulates the processes of root hair development, leaf phyllotaxy, vascular development of cotyledons, lateral root formation, and apical hook formation (Swarup and Péret, 2012).

Apolar and long-distance transport of auxin is largely maintained through the efflux activities of P-glycoproteins in the ABCB transporter class, including ABCB1, ABCB4, and ABCB19 (Geisler and Murphy, 2006; Kang et al., 2011; Henrichs et al., 2012; Ruiz Rosquete et al., 2012). Instead of maintaining proper development and growth through PAT, these transporters are implicated in non-polar transport due to their localization (Geisler et al., 2005). However, interactions with PINs has been suggested as a means of chaperoning localization to direct their transport flows in a polarized manner (Bandyopadhyay et al., 2007; Blakeslee et al.,

2007). Even when unaccompanied by PINs, ABCB transport of auxin is dependent upon and modulated by other interactions. TWD1, a member of the FK506 binding protein family, is a required interaction partner with ABCBs at both the plasma and vacuolar membranes for transport activity. Knockout *twd1* mutants display a “twisted dwarf” phenotype indicative of auxin mis-regulation caused by reduced auxin transport via ABCB transporters (Kamphausen et al., 2002; Bailly et al., 2008; Wu et al., 2010; Henrichs et al., 2012).

In addition to protein-protein complexes, auxin transport via ABCBs is regulated by endogenous flavonols. These secondary metabolites were first discovered to regulate auxin transport through experiments identifying molecules competing with the known auxin transport inhibitor, N-1-Naphthylphthalamic acid (NPA) (Jacobs and Rubery, 1988). Since then, kaempferol and quercetin have been shown to physically interact with and inhibit the auxin efflux activity of the TWD1/ABCB1 complex (Bailly et al., 2008). However, the relative effects of each class of flavonol appear to be tissue specific. Extensive research has provided evidence of a strong effect of quercetin on Arabidopsis root tissues (Murphy et al., 2000; Brown et al., 2001; Grunewald et al., 2011), while kaempferol derivatives have shown to inhibit auxin transport in shoots, independent of quercetin (Yin et al., 2014).

DICAMBA HERBICIDE

Overview and Mode of Action

Auxin-mimicking compounds were the first discovered synthetic herbicides (Sterling and Hall, 1997). Since its commercial introduction fifty years ago, dicamba has been widely used in agriculture. Its selective activity to control eudicots in cereal crops has been a valuable tool for weed management (Grossmann, 2010). Dicamba is classified as a synthetic auxin hormone

mimic due to physiological and morphological similarities with indole-3-acetic acid (IAA), a highly abundant endogenous auxin (Grossmann, 2010). It is known to interact with well-characterized auxin receptors (Gleason et al., 2011). Growth effects are dose-dependent and include stem curling, tissue swelling, leaf epinasty, and stunted growth, while physiological effects include stomatal closure and reduced transpiration, reduction of carbon fixation and central metabolism, and production of reactive oxygen species (Abel and Theologis, 1996; Kelley and Riechers, 2007; Grossmann, 2010; Sauer et al., 2013; Christoffoleti et al., 2015). Massive changes in gene regulation leads to ethylene and abscisic acid biosynthesis. These hormones initiate senescence, leading to both cellular and whole-plant death (Grossmann, 2010).

Dicamba Resistance

Beginning in 1990, twenty-three years after its commercial introduction, fourteen unique cases of field-evolved dicamba-resistant weed populations have been documented worldwide (Heap, 2016). While genetics studies have identified Mendelian inheritance patterns for some resistance cases (Jasieniuk et al., 1995; Preston et al., 2009), the molecular bases of these field-evolved phenotypes remain elusive. In contrast to field-evolved cases of dicamba-resistant weedy species, investigations of mutant *Arabidopsis thaliana* have provided insights into the complex activity of dicamba. Gleason et al. (2011) discovered that F-Box proteins TIR1 and AFB5 were both targets of dicamba. Reduced root growth sensitivity to dicamba in both *tir1-1* and *afb5* lines as well as the additive resistance observed in the double-mutant *tir1-1/afb5* suggest dual roles in dicamba perception. However, Walsh et al. (2006) found that *afb5-4*, a mutant with a different mutation within the same auxin receptor was reported to display 50-fold resistance to the picolinate auxin clopyralid, but showed no resistance to dicamba, an analog of

the aryloxyacetate auxin, fluroxypyr, or 1-naphthylacetic acid. These two studies suggest that AFB5 is a receptor of both dicamba and clopyralid with unique non-synonymous substitutions causing different conformational changes to the protein's binding pocket, each of which leads to the exclusion of different auxinic herbicide compounds.

In addition to mutant analyses, genetic engineering efforts have successfully produced dicamba-resistant transgenic plants. A novel, three-component enzyme capable of converting dicamba into 3,6-dichlorosalicylic acid through *O*-demethylation of has been isolated from the soil bacterium, *Pseudomonas maltophilia* Strain DI-6 (Wang et al., 1997; Herman et al., 2005). This dicamba metabolism system has been engineered into two species with naturally low dicamba tolerances: *Arabidopsis thaliana*, tomato, tobacco, and soybean (Behrens et al., 2007). Maize, a monocot with elevated tolerance to dicamba compared to dicots, has also been transformed with the dicamba *O*-demethylase system (Cao et al., 2011). Transgenic maize lines display more robust dicamba tolerance, enabling higher crop safety and a wider developmental window of safe dicamba field applications (Cao et al., 2011). These transgenic cases provide evidence of a unique type of metabolism-based dicamba resistance, an unreported mechanism of resistance in wild populations of weedy species to-date.

In total, fourteen cases of dicamba resistance have been documented (Heap, 2016), but the mechanisms of resistance largely remain mysteries. Few resistant populations have been investigated further than establishing significantly reduced sensitivity to dicamba application via dose response bioassays. While inheritance patterns have been identified for some phenotypes (Jasieniuk et al., 1995; Preston et al., 2009), conclusive evidence of specific resistance mechanisms from physiological and molecular experiments remains elusive.

In 1990, a population of wild mustard (*Sinapis arvensis*) infesting spring barley and wheat cropping systems was identified as dicamba-resistant in addition to other auxinic herbicides: 2,4-D, dichlorprop, MCPA, mecoprop, and picloram (Heap and Morrison, 1992). This population has been extensively characterized to understand the inheritance, physiology and putative mechanisms of dicamba resistance. Jasieniuk et al. (1995) identified that the dicamba resistance phenotype of this population is inherited as a single gene, completely dominant nuclear allele. Further work failed to identify physiological evidence suggesting a mechanism of resistance due to the lack of differences in dicamba absorption, translocation, or metabolism in the resistant population compared to susceptible individuals (Peniuk et al., 1993). In light of these findings, Hall et al. (1993) quantified ethylene production in response to dicamba treatment, identifying a significantly greater generation of ethylene in the susceptible compared to resistant individuals, a finding which they conjecture resulted from differential dicamba perception caused by mutation of an auxin binding protein of unknown identity. Further support of this hypothesis was found by investigating the effect of dicamba application after pretreatments with either calcium or verapamil, a calcium channel blocker. Results showed that dicamba had a decreased inhibition of root growth when individuals were pretreated with calcium, while pretreatment with verapamil increased susceptibility to dicamba (Wang et al., 2001). While these experiments fail to identify genes conferring dicamba resistance, they confirm the role of calcium-mediated auxin signaling in the resistant response. Further work has characterized the binding affinity of ABP for ³H-IAA, identifying a low- and high-affinity binding sites in the susceptible biotype, but only a low-affinity binding site in the resistant biotype (Mithila and Hall, 2005). This finding suggests that high-affinity binding of ABP to auxinic molecules is required for herbicidal efficacy. Cell elongation studies comparing resistant

and susceptible wild mustard cell elongation to ABP1 antisense- and wild type tobacco cell elongation found significant biotype \times treatment effect for both the wild mustard and tobacco, providing further evidence that ABP activity may be responsible for stimulation of cell elongation and the resistance phenotype (Mithila and Hall, 2005). However, evidence confirming ABP's role in wild mustard resistance to auxin molecules remains inconclusive.

Beginning in 1990, eight unique cases of field-evolved dicamba-resistant *K. scoparia* populations have been identified worldwide (Heap, 2016). The inheritance pattern for one documented phenotype has been identified (Preston et al., 2009). Physiological experiments identified significantly reduced ethylene production in the resistant line compared to susceptible (Belles, 2004), but no mechanisms of resistance have been confirmed. Various physiological experiments have found that resistant populations lack significant differences in absorption, translocation, and metabolism of dicamba compared to susceptible populations (Cranston et al., 2001). This lack of evidence for non-target site mechanisms of resistance and further studies identifying reductions in shoot gravitropism (Goss and Dyer, 2003) have led to speculations that differences in auxin-receptor proteins such as ABP, TIR1, AFBs, and SKP2A could confer the dicamba-resistance phenotype. Studies of transcriptional regulation have identified differentially expressed transcripts in response to dicamba treatment (Cranston et al., 2001), including a number related to ethylene biosynthesis. However, whether this pattern of transcription confers resistance or results from the resistance mechanism remains uncharacterized.

CHAPTER 2: UNDERSTANDING DICAMBA RESISTANCE IN *KOCHIA SCOPARIA* – A FUNCTIONAL GENOMICS APPROACH

INTRODUCTION

Kochia scoparia is an annual, herbaceous weed native to Eurasia with high rates of outcrossing due to protogynous monoecious flowers. Prolific seed production along with high outcrossing rates results in large, highly genetically diverse wild populations. Since its introduction to North America as an ornamental species in the mid- to late 1800s, it has escaped cultivation and become one of the most common weeds of cultivated lands in the western high plains (Friesen et al., 2009).

Herbicides have been used extensively to manage wild *K. scoparia* populations, and evolution of herbicide-resistance has occurred repeatedly. To date, 54 wild populations of *K. scoparia* have been documented with resistance to 24 distinct molecules comprising four unique herbicide modes of action including inhibition of Photosystem II, inhibition of Acetolactate Synthase, inhibition of 5-enol-pyruvylshikimate-3-phosphate synthase (EPSPS) and synthetic auxins (Heap, 2016).

With regard to synthetic auxins, eight populations of *K. scoparia* have evolved resistance to this mode of action. One such resistant population from Henry, NE was characterized as resistant to dicamba. The mode of inheritance for this phenotype has been characterized as resulting from a single, dominant gene (Preston et al., 2009). However, the molecular genetic resistance mechanism of this phenotype remains unknown. Therefore, the aim of this research was to identify the molecular basis of the dicamba-resistance phenotype of this population of *K. scoparia*.

METHODS

Characterization of Lines

Dicamba Dose Response

Two genetically distinct, inbred *K. scoparia* lines known as 7710S (dicamba-susceptible) and 9425R (dicamba-resistant) (Preston et al., 2009) were used in this experiment. These lines were derived by single-seed descent for four generations followed by bulk seed production within lines for 13 generations. Seeds of 7710S and 9425R were planted in germination flats and transferred to 18-insert flats (8 x 8 cm pots) filled with custom blend potting mix (Fafard, Sun Gro Horticulture, Agawam, MA, USA), and grown in a greenhouse at 23°C, 14 hr light/ 10 hr dark photoperiod. Emerged individuals were grown to a size of 7 cm (approx. 6 weeks) and 18 individuals per line were treated with each of following dicamba doses (all dicamba applications used the commercial formulation Clarity): 0, 11.2, 56, 280, 1400, 7000, or 14000 g a.e. ha⁻¹ at an application volume of 187 L ha⁻¹. Applications were made using a XR TeeJet 11008 VS nozzle from a height of 40 cm using a cabinet spray chamber (DeVries Generation III Research Sprayer). Shoot height of each individual was measured at the time of application and two weeks after treatment. Eighteen individuals were measured at each dose and the experiment was conducted twice, for a total of thirty-six individuals of each line at each dose.

Statistical Analysis

The difference in shoot height for each individual was assessed as a relative percentage of the mean shoot growth of all 36 untreated individuals from the corresponding line. The relative percentage value was used as the response variable. Data for each line were fit to a four-parameter log-logistic model:

$$Y = c + \frac{d - c}{1 + \exp [b(\log x - \log e)]}$$

Where d is the upper limit, c is the lower limit, e is the GR_{50} (dose causing a 50% reduction in plant growth), and b is the relative slope around e using the ‘drc’ package (Ritz and Streibig, 2005) in the R statistical computing language (R Core Team, 2016). The difference between GR_{50} estimates was compared with a t-test (Knezevic et al., 2007) and the relative difference was expressed as a ratio of 9425R to 7710S.

RNA-Seq

Plant Material

Eight R and S individuals were grown in 8 × 8 cm pots filled with custom blend Farfard potting soil in the greenhouse. About two months after sowing, these individuals reached a shoot height of 7 cm. Four individuals each of R and S were then treated with 280 g a.e. dicamba ha⁻¹ using an application volume of 187 L ha⁻¹. The treatment was applied in a cabinet spray chamber (DeVries Generation III Research Sprayer) from a height of 40 cm using a XR TeeJet 11008 VS nozzle. Treated plants were returned to the greenhouse and at 12 hours after treatment, plant tissue was sampled from all sixteen individuals, consisting of four untreated 9425R individuals, four untreated 7710S individuals, four treated 9425R individuals, and four treated 7710S individuals. The three smallest expanding leaves (approx. 30mg) from the apical meristem of each individual were collected, placed in a 2 mL tube, and immediately flash frozen in liquid nitrogen. Tissues were stored at -80°C.

Plant tissue was ground to a fine powder in 2 mL tubes with polypropylene micropestles (tissues remained frozen during disruption). Total RNA was then extracted from the ground tissue using the Qiagen RNeasy Plant Mini kit following the manufacturer’s protocol with minor

modifications. Buffer RLT was utilized followed by a 2-minute incubation at 56°C, and 50 µL RNase-free water was used for final elution. Immediately after elution, yield and purity were measured with a NanoDrop 2000 spectrophotometer. RNA integrity (RIN) was measured using a 2 µL aliquot of each RNA extraction with an Agilent 2100 Bioanalyzer using the Plant RNA Nano assay. Quality scores for all samples met or exceeded a RIN score of 9.2. Following quality control assays, all samples were treated in solution with Qiagen RNase-Free DNase Set to remove contaminating DNA.

Alignment and Differential Expression

Strand specific RNA-seq libraries were prepared from RNA samples using the Illumina TruSeq Stranded Total RNA Library Prep kit. Libraries were prepared for 100 nucleotide paired-end sequencing from fragments with an average length of 250 nucleotides (80-500nt). All 16 libraries were barcoded, multiplexed, and sequenced in parallel on 4 lanes of an Illumina HiSeq 2500 flow cell, yielding 1.9 billion paired-end reads. Individual library yields ranged from 55.7 million to 63.4 million paired reads. Quality scores for all sequenced nucleotides equaled or exceeded 99.9% confidence (Q30 Phred score, ASCII offset 33).

A modified version of the *de novo* reference transcriptome generated by Wiersma et al. (2014) was used for this experiment. For each predicted gene locus, only the contig containing the longest predicted open reading frame as predicted by TransDecoder was retained. This resulted in a 36-Mb transcriptome with 41% GC content contained in 34,933 contigs with an N50 contig size of 1,749. Putative annotations were assigned for contigs based upon the identity of BLASTx (Camacho et al., 2009) hits. Putative annotations were assigned to 14,223 contigs (40.7% of total reference) based upon matches to the TAIR10 protein database (Berardini et al.,

2015). Of the remaining contigs, 14,940 (42.7% of total reference) were annotated using the UniProt database (Bateman et al., 2015), and 5,770 (16.5% of total reference) had no matches.

Reads were aligned to a reference transcriptome using the Bowtie2 short read aligner (Langmead and Salzberg, 2012). All possible end-to-end alignments were identified using the “very-sensitive” preset option of Bowtie2. The majority (70%) of reads aligned concordantly (paired reads aligning in the expected orientation) once, <1% of reads aligned concordantly more than once, and 29% of reads did not align concordantly. Only aligned reads with a MAPQ score ≥ 30 were retained for downstream analysis. The SAMtools function “idxstats” (Li et al., 2009) was used to extract raw read counts for each transcript in the reference. The data were further analyzed with edgeR (Robinson et al., 2009), which uses a negative binomial distribution, estimates dispersions by conditional maximum likelihood, and assesses differential expression with an exact test adapted for overdispersed data. Transcripts were only considered expressed if at least 2 libraries met or exceeded 1 count-per-million (CPM). Unexpressed transcripts were eliminated from downstream analysis. The “calcNormFactors” function computed “effective library size” for each sample, which accounts for RNA composition – the relative proportion of a library represented by very highly expressed genes, which may cause under-sampling of more lowly expressed genes. The data were analyzed by fitting the negative binomial generalized linear model (GLM), “ $Y = \text{Line} + \text{Treatment} + \text{Line} * \text{Treatment}$ ”, with calculated Cox-Reid dispersion estimates to account for technical and biological variance in the data. Finally, each term in the GLM was assessed for differentially expressed transcripts using a likelihood ratio test with the following cutoff criteria: \log_2 fold-change in expression ≥ 2 , and False Discovery Rate (FDR) adjusted p-value ≤ 0.05 .

In order to focus only on transcripts differing between lines in response to dicamba, significantly differentially expressed transcripts identified by the interaction term, “Line*Treatment” were selected for further investigation. The selected transcripts were assessed for overrepresented keywords associated with their ortholog annotations from the *Arabidopsis thaliana* database using GeneCloud software (Krouk et al., 2015). Additionally, the same set of transcripts was used to generate a clustered heatmap to identify clusters of transcripts with similar expression trends.

These transcripts were clustered into expression profiles. The appropriate number of K-means clusters to be used for clustering was identified as k=21 according to Silhouette Width determined by the “clValid” package in R (Brock et al., 2008). Mean log₂CPM expression values for each experimental modality were clustered into 21 K-means clusters using the “pheatmap” package in R (Kolde, 2015). Each unique cluster was individually tested for enrichment of transcript annotation keywords using GeneCloud software to identify keywords and processes related to expression trends among significant transcripts. The combined dataset of keyword enrichment with expression profile clustering was interpreted using physiological evidence to identify transcripts of interest for further investigation and expression validation.

SNP Genotyping from RNA-Seq Alignments

Consensus sequences for both 7710S and 9425R were produced using RNA-seq alignment data from all eight individuals of each line. The SAMtools function ‘mpileup’ (Li et al., 2009) extracted summary information from all eight alignment files per line, a call for each base was made using the BCFutils function ‘call’, and VCFutils was implemented to convert the data to a fastq file. In addition, putative peptide sequences were determined from fastq data files

for known auxin receptors: ABP1, TIR1, AFB3, AFB5, and SKP2A as well as the auxin transporters: PIN3, PIN4, PIN5, AUX1, LAX2, ABCB1, ABCB19. Peptides were determined by extracting the amino acid sequence of the longest open reading frame for each line as determined using the ExPASy Translate tool (Artimo et al., 2012). Consensus sequences for 9425R and 7710S lines were then compared to identify SNPs using the Needleman-Wunsch alignment algorithm in EMBOSS (Rice et al., 2000).

Validation of in silico Candidate Expression via qRT-PCR

In silico differential expression results from RNA-seq were experimentally evaluated with qRT-PCR. Aliquots of the same RNA samples used for RNA-seq were used for this assay (see tissue sampling from RNA-seq). For all samples, 1 µg of RNA was treated with DNase I (Thermo Scientific) according to manufacturer instructions, immediately followed by first-strand cDNA synthesis with qScript™ cDNA Synthesis Kit (Quanta Biosciences), primed by both random hexamer and oligo-dT primers.

Seven genes with the following annotations: Acetolactate Synthase (ALS), Sucrose Non-Fermenting 1 (SNF1), Cullin 1 (CUL1), Actin-1, CCG Binding Protein 1 (CBP1), Peroxidase 2 (PERX2), and Exocyst Complex Component SEC5 (SEC5) were evaluated for utility as normalization genes in qRT-PCR based on transcription stability measured with CPM and scored by coefficient of variation. Expression was measured in RNA from 7710S and 9425R shoot apical meristematic tissues under untreated and dicamba-treated conditions (n=12) using a CFX Connect™ Real Time PCR Detection System (Bio-Rad) and C_T stability was assessed with BestKeeper (Pfaffl et al., 2004). ALS, Actin-1, and SEC5, the three primer sets with the lowest

standard deviation of C_T : 0.48, 0.46, and 0.50, respectively, were chosen as qRT-PCR normalization genes.

Relative expression of CHS, F3'H, and FLS was assayed by qRT-PCR. All reactions were performed in duplicate and for each primer set, a reaction with no template cDNA was used as a negative control. Each reaction contained a 20 μ L volume consisting of 10 μ L PerfeCTa SYBR Green Fastmix (Quanta Biosciences), 2.5 μ L of 1:20 diluted cDNA, 1 μ L of primers (1:1 mixture of forward and reverse primers (Table 1) at 10 μ M each), and 6.5 μ L of distilled, nuclease-free water. Thermal cycling of samples included a 15-minute incubation step at 95°C followed by 35 cycles 95°C for 30 sec and 60°C for 1 min. A melt curve analysis followed cycling to confirm the presence of a single product for each reaction. Relative expression of target transcripts was calculated using a modified version of the $2^{\Delta C_t}$ method wherein $\Delta C_T =$ [geometric mean of normalization genes Actin-1, ALS, and SEC5 C_T 's – gene of interest C_T]. All primers were empirically determined to have amplification efficiency between 90 and 110%, confirming the equivalent efficiencies required to calculate relative expression using the $2^{\Delta C_t}$ method (Livak and Schmittgen, 2001; Schmittgen and Livak, 2008).

Hypothesis Testing: Forward Genetics

Quantification of differential expression with RNA-seq led to the hypothesis that increased transcription of the flavonol biosynthesis pathway is increasing the quantity of the auxin transport-inhibiting flavonol compounds quercetin and kaempferol. This hypothesis was tested using the following methods.

Breeding

Relative transcription values validated with qRT-PCR were evaluated using a forward genetics approach with an F₂ population produced from 7710S and 9425R lines. The dicamba-resistant phenotypes of all 9425R individuals used in crosses were confirmed by survival after 1× dicamba treatment (280 g a.e. ha⁻¹). Susceptibility of 7710S was not confirmed with treatment due to the lethality of phenotype validation. Twelve individuals of both 9425R and 7710S lines were allowed to cross-pollinate in an enclosed pollination chamber with directional airflow. Due to the dominant, single-gene Mendelian inheritance of the dicamba-resistance phenotype, all 7710S flowers pollinated by 9425R produce dicamba-resistant individuals (Preston et al., 2009). Putative F₁ seeds were collected from 7710S parental individuals and treated with a 1× application of dicamba to confirm successful crossing with 9425R pollen. Surviving F₁ individuals were self-pollinated and F₂ seed was collected. Mendelian, 3:1 segregation of resistant to susceptible phenotypes in the F₂ population was confirmed with a 2× application of dicamba (560 g a.e. ha⁻¹). 7710S and 9425R individuals were used as positive controls for classification of resistant and susceptible F₂ phenotypes in response to dicamba application.

Relative Expression Quantification

Leaf tissue from the shoot apical meristem (~30mg) was collected twelve hours after treatment with 560 g a.e. ha⁻¹ dicamba, flash frozen in liquid nitrogen and stored at -80°C until disruption using a TissueLyser II (Qiagen). Dicamba-R (F₂R) and dicamba-S (F₂S) F₂ individuals were identified at 14 days after treatment, and these individuals were selected for total RNA extraction from disrupted tissues using the TRIzol (Invitrogen) method and relative expression

quantification of CHS, F3'H, and FLS was conducted as described above (see RNA-seq Validation).

CHS Copy Number Quantification

Fresh tissue was collected from the lowest fully-expanded leaf of the same F₂R and F₂S individuals sampled for relative expression quantification assays. DNA was extracted from frozen tissue using the CTAB method. Relative CHS:ALS genomic copy number was quantified for each individual. Reactions were performed in duplicate and for each primer set, a reaction with no template genomic DNA was used as a negative control. Each reaction contained a 20 μ L volume consisting of 10 μ L PerfeCTa SYBR Green Fastmix (Quanta Biosciences), 4 μ L of 5 ng/ μ L genomic DNA, 1 μ L of primers (1:1 mixture of forward and reverse primers at 10 μ M each), and 5 μ L of distilled, nuclease-free water. Thermal cycling of samples included a 15-minute incubation step at 95°C followed by 35 cycles 95°C for 30 sec and 60°C for 1 min. A melt curve analysis followed cycling to confirm the presence of a single product for each reaction. Relative CHS:ALS genomic copy number was calculated using the 2 ^{Δ C_T} method wherein Δ C_T = [ALS C_T – CHS C_T] (Schmittgen and Livak, 2008).

RESULTS

Characterization of Lines: Dicamba Dose Response

Dicamba response phenotypes of both inbred lines were characterized with a dose response experiment (Figure 1, Figure 2). The four-parameter log-logistic models fit for each line demonstrate significantly different responses to dicamba treatment [9425R: $f(x) = 1.75 + (105.79)/(1 + e^{1.2(\log(x) - \log(1.51))})$), GR₅₀ = 84 g a.e. dicamba ha⁻¹; 7710S: $f(x) = -0.21 +$

$(98.62)/(1+e^{1.93(\log(x)-\log(0.3))})$, $GR_{50} = 427$ g a.e. dicamba ha^{-1}]. 7710S displayed more pronounced epinasty and senescence at lower doses of dicamba than 9425R. Additionally, the ratio of GR_{50} values shows 5× resistance to dicamba in 9425R compared to 7710S (Table 2). The significant phenotypic differentiation between lines provides grounds for RNA-seq investigation of differential gene expression in response to dicamba treatment.

RNA-seq

Differential Expression

A principle components analysis (PCA) of whole-transcriptome expression profiles for all 16 individuals shows primary differentiation of the data by genetic background, while individuals are secondarily differentiated by treatment (Figure 3). All 7710S individuals cluster positively according to Principle Component 1 (PC 1) while 9425R individuals cluster with negative values. Additionally, dicamba-treated individuals cluster negatively according to Principle Component 2 (PC 2) whereas untreated controls cluster positively. The distinct clusters of replicates within all four experimental modalities suggests whole-transcriptome consistency among biological replicates. A Venn diagram (Figure 4) displaying significant transcripts identified by each term of the generalized linear model confirms the primary effect of genetic background (1,449 total transcripts) and secondary effect of experimental treatment (717 total transcripts) predicted by PCA with regard to significant differential expression. In an effort to understand the significant differences in expression between 9425R and 7710S in response to dicamba treatment, the significantly differentially expressed transcripts identified by the GLM interaction term, “Line*Treatment” were chosen for further analysis.

A total of 386 transcripts were identified as significantly differentially expressed by the interaction term. Keyword enrichment of transcript annotations in this list were assessed for overrepresentation in the dataset (Figure 5). Identified keywords included biotic and abiotic stress and signaling, resistance, transport, and movement. Identification of these keywords is expected, given the known cross-talk between auxin signaling and biotic-stress response pathways.

Auxin Receptor and Transporter SNPs

The *in silico* genotyping of well-characterized auxin receptors: ABP1, TIR1, AFB3, AFB5, and SKP2A as well as the auxin transporters: PIN3, PIN4, PIN5, AUX1, LAX2, ABCB1, ABCB19 found no non-synonymous SNPs between 9425R and 7710S for any of these transcripts (Table 3). The lack of SNPs suggests that the differential dicamba-response phenotypes of 9425R and 7710S are not due to differences in dicamba perception or transport coming from truncated proteins or point-mutations causing conformational changes in any of these proteins.

Hypothesis Generation

Dicamba translocation experiments with 9425R using ¹⁴C radiolabeled dicamba treatments have demonstrated reduced acropetal and basipetal translocation of dicamba from the site of application compared to susceptible lines (M. Jugulam, Kansas State University, personal communication). This evidence suggests that 9425R may exhibit reduced dicamba loading into both xylem and phloem or vacuolar sequestration. Additionally, dicamba was not differentially metabolized in 9425R and 7710S (M. Jugulam, Kansas State University, personal

communication). These findings suggest both that the distinct dicamba response phenotypes of these two lines are not differentiated by dicamba detoxification through metabolism. It also suggests that dicamba conjugation to a sugar, glutathione, or amino acid is not necessary for the reduced dicamba translocation observed in 9425R.

In light of this physiological evidence regarding reduced dicamba translocation, each cluster of transcripts in the clustered heatmap (Figure 6) identified by the GLM interaction term were investigated for enriched keywords with links to xenobiotic transport or sequestration including: “membrane”, “movement”, “transport(er)”, “vacuole”, and “wall”. Cluster B revealed Flavonoid 3'-Hydroxylase (F3'H, *TRANSPARENT TESTA 7*), the enzyme responsible for determining the ratio of quercetin to kaempferol derivatives in the flavonoid biosynthetic pathway (Figure 7). The reduced dicamba translocation observed in 9425R (M. Jugulam, Kansas State University, personal communication) and the identification of the flavonoid pathway with differential expression analysis suggests that flavonoid metabolites may be responsible for reducing the transport of dicamba in 9425R compared to 7710S. Both quercetin and kaempferol metabolite classes are known modulators of auxin transport and vascular loading (Jacobs and Rubery, 1988; Murphy et al., 2000; Brown et al., 2001; Buer and Muday, 2004; Geisler and Murphy, 2006; Morris and Zhang, 2006; Peer and Murphy, 2007; Zhao and Dixon, 2010). Further investigation of the flavonoid biosynthesis pathway revealed pairwise expression differences in Chalcone Synthase (CHS, *TRANSPARENT TESTA 4*), Chalcone Isomerase (CHI, *TRANSPARENT TESTA 5*), and Flavonoid 3-Hydroxylase (F3H, *TRANSPARENT TESTA 6*). All were significantly upregulated in 9425R compared to 7710S under dicamba-treated conditions (Figure 8), suggesting greater metabolic flux through the flavonoid biosynthesis pathway in 9425R compared to 7710S. This proposed increase in expression would lead to higher quercetin

and kaempferol derivative concentrations and may reduce dicamba translocation in both basipetal and acropetal directions through reduction or inhibition of intercellular transport and vascular loading via known auxin transporters ABCB1, ABCB4, or ABCB19 (Di Pietro et al., 2002; Geisler and Murphy, 2006; Morris and Zhang, 2006; Blakeslee et al., 2007; Bailly et al., 2008). Notably, no differences in transcription were identified among ABCB1 or ABCB19 *in silico* (Figure 9). No transcripts annotated as ABCB4 exceeded 500 nucleotides and were not analyzed.

Hypothesis Validation

qRT-PCR Validation of in silico Candidate Expression

RNA-seq expression values were validated with qRT-PCR relative expression assays using the $2^{\Delta CT}$ method (Schmittgen and Livak, 2008). Quantitative transcription values from RNA-seq (CPM) for each transcript were divided by the geometric mean of the same housekeeping genes used in qRT-PCR and thus expressed as relative values comparable to the $2^{\Delta CT}$ method. Values generated with each method were plotted on separate axes and linear regressions were fit to the mean expression value of each experimental modality for WRKY23, CHS, F3'H, and FLS (Figure 10). The linear regression using all transcripts and experimental modality means showed high correlation of the two methods ($Y = 2.016 * X - 0.1597$; $R^2 = 0.83$), suggesting consistency of transcription quantification both *in silico* and via qRT-PCR techniques.

Three key enzymes in the flavonoid biosynthesis pathway were chosen for validation, including the rate-limiting step, CHS; the enzyme responsible for determining the ratio of kaempferol to quercetin derivatives, F3'H; and the enzyme responsible for converting

dihydroflavonols to their active flavonol forms, FLS. CHI and F3H were excluded from validation due to their lesser roles in determining the overall metabolic flux through the pathway compared to CHS and their lack of impact on the relative output of various flavonoid metabolite classes. CHS, F3'H, and FLS were assessed for transcription level expression in the same total RNA samples used for RNA-seq. Expression of each transcript was analyzed with a two-way ANOVA to test for effects of "line", "treatment", and "line*treatment". F3'H displayed a significant "line*treatment" effect ($p=0.04$) (Figure 11.B) and FLS showed no significant effect of "line", "treatment", or "line*treatment" (Figure 11.C). Importantly, CHS displayed a significant effect of "line" ($p=0.004$), suggesting a constitutive expression difference between 9425R and 7710S. Constitutive CHS expression difference between 9425R and 7710S was confirmed with a t-test with Welch's correction ($p=0.01$) comparing all eight individuals (control and dicamba-treated conditions together) of each line (Figure 11.A). This difference in expression suggests increased flux through the flavonoid biosynthetic pathway in 9425R compared to 7710S and greater quantities of kaempferol and quercetin, which could be reducing dicamba efficacy by inhibiting its translocation.

Differential gene expression between biotypes may be explained by genomic copy number variation (Gaines et al., 2010). To address this possible cause of increased CHS transcription in 9425R compared to 7710S, genomic copy number of CHS was calculated relative to ALS using qPCR. Relative CHS:ALS copy numbers of 9425R and 7710S were observed as 0.96 and 1.12, respectively. (Figure 12). This finding confirms that duplication of the CHS locus in 9425R has not occurred and thus does not explain the increased transcription of CHS compared to 7710S. However, undiscovered *cis*- or *trans*-acting elements may confer the observed difference in CHS transcription between 9425R and 7710S.

Forward Genetics: Candidate Expression and CHS Copy Number

Previously established single-gene, dominant Mendelian inheritance of the dicamba-resistance phenotype was confirmed with forward genetics phenotyping using an F_2 population derived from a self-pollinated F_1 cross between 9425R σ^7 and 7710S ♀ . F_2 individuals were visually assessed as resistant or susceptible in response to dicamba treatment using lines 9425R and 7710S as positive controls for resistant and susceptible phenotypes, respectively. The 3:1 ratio of resistant to susceptible individuals in the F_2 population demonstrated by Preston et al. (2009) was confirmed with a chi-squared test for goodness of fit (Table 4). Candidate transcript upregulation was tested for co-segregation with the resistance phenotype in this segregating F_2 population.

CHS, F3'H, and FLS were chosen for qRT-PCR relative expression quantification in dicamba-resistant F_2 individuals (F_2R) and dicamba-susceptible F_2 individuals (F_2S) using RNA extracted from apical meristematic tissues twelve hours after dicamba treatment (Figure 13). F3'H, which was predicted to have greater expression in F_2R showed significantly greater expression in F_2S ($p = 0.001$, Welch's unpaired t-test), suggesting that the expression profile observed in 9425R is not responsible for the resistance phenotype. Importantly, F_2R individuals displayed consistent and significant upregulation of CHS compared to F_2S individuals ($p = 0.0004$, unpaired t-test with Welch's correction), confirming the expression profile segregation predicted by RNA-seq and confirmed with qRT-PCR. These findings suggest that while the relative abundance of kaempferol to quercetin does not confer resistance, increased flavonoid biosynthesis may

DISCUSSION

RNA-seq: Conclusions

Physiological evidence identified no difference in dicamba metabolism between 9425R and 7710S lines, and a significantly lower translocation of dicamba in 9425R compared to 7710S suggesting that reduced capacity for translocation of dicamba could be involved the resistance phenotype of 9425R (M. Jugulam, Kansas State University, personal communication). As such, significantly differentially expressed transcripts identified by RNA-seq were investigated for transcripts related to intracellular sequestration, intercellular transport, and vascular loading of endogenous auxin, indole-3-acetic acid (IAA), given dicamba's auxin-mimic mode of action (Grossmann, 2010).

CHS was identified as a candidate gene due to its role in the biosynthetic pathway of the flavonols quercetin and kaempferol. In addition to their anti-oxidant activities (Keilig and Ludwig-Mueller, 2009; Nakabayashi et al., 2014), quercetin and kaempferol are known inhibitors of auxin transport in both root tissues (Grunewald et al., 2011; Kuhn et al., 2011; Kuhn et al., 2016) and shoot tissues (Ringli et al., 2008; Yin et al., 2014) where they interact with ABCB proteins known to transport auxin. Further investigation of the flavonoid biosynthesis pathway showed constitutive and post-treatment upregulation of CHS, CHI, and F3H in 9425R compared to 7710S (Figure 12). CHS and F3'H were chosen for forward genetics validation due to their key roles as the rate-limiting step in flavonoid biosynthesis and determinant of the ratio of quercetins to kaempferols. Expression of these two transcripts with qRT-PCR in an F₂ population segregating for resistance identified significantly higher expression of CHS in F₂R individuals compared to F₂S individuals. This co-segregation of the resistance phenotype with upregulated CHS associates the dicamba-resistance phenotype to a higher metabolic flux through

the flavonoid pathway (Figure 13). Greater flavonoid pathway biosynthetic flux should lead to increased production of kaempferol and quercetin, which are known to inhibit intercellular transport and vascular loading of auxin. Thus dicamba movement may also be reduced by this mechanism, inhibiting translocation to sensitive meristematic tissue and conferring the observed resistance phenotype.

The lack of differential dicamba metabolism in the physiological data and the significant reduction of dicamba translocation strongly supports the present hypothesis of dicamba transport reduction caused by increased production of flavonol metabolites. The forward genetics approach of this study provides evidence that the resistance phenotype is inherited with upregulation of CHS compared to the susceptible phenotype. Although this provides an association between expression and phenotype, the evidence is far from conclusive. This hypothesis requires further genetic evidence and quantification of flavonol metabolites to implicate their role in the reduction of dicamba transport.

Further Work: Mutant Analysis, Analytical Chemistry, and Mapping

Further confirmation of the relationship between phenotype and expression pattern will include experiments using *Arabidopsis thaliana*. A CHS knockout line of *A. thaliana* will provide the necessary tool to isolate and implicate individual genes in the resistance phenotype. A dose response experiment will isolate the effect of this gene knockout compared to the wild type genetic background and assess the impact of CHS on dicamba-resistance. If the proposed hypothesis holds true, the knockout mutant should display increased susceptibility to dicamba compared to wild type. Additionally, an *Arabidopsis* line transformed with a copy of the CHS gene preceded by a constitutive overexpression promoter should display increased resistance

compared to the wild type. The results of these two dose response experiments will either disprove the hypothesis or provide it with strong molecular genetic support necessary to justify further experimentation.

While lines of CHS knockout and overexpressing lines may provide evidence to suggest a role for CHS in dicamba-resistance, these experiments lack the power to implicate the role of quercetins and kaempferols in inhibition of dicamba transport. As such, if the proposed *Arabidopsis* dose responses support the hypothesis that increased quantities of quercetin and kaempferol reduce dicamba transport, quantification of these two metabolites will be necessary. Although undetected in the reference transcriptome or RNA-seq analysis and therefore unmeasured, increased activity of Dihydroflavonol 4-Reductase (DFR) could shunt flux toward tannin and anthocyanin biosynthesis, reducing the production of kaempferol and quercetin (Figure 7). As such, quantification of the metabolites will be necessary to account for unmeasured gene expression which could confound the current hypothesis. Quantification of implicated auxin-transport modifying flavonol conjugates in 9425R, 7710S, F₂R, and F₂S will enable a correlation of phenotype with metabolite profile. This experiment, building on the molecular genetic evidence provided by the CHS knockout and overexpression lines, will provide further evidence required to implicate the role of flavonols on the dicamba resistance phenotype.

Finally, as a complement to the RNA-seq experiment, a genome mapping experiment will identify regions of the *K. scoparia* genome associated with the resistance phenotype of 9425R. While currently in progress, assembly of the *Kochia* genome has reached sufficient quality to enable genome-wide association studies. Sequencing following genome complexity reduction produces thousands of SNP loci, which when aligned to the genome reference will be utilized to

identify genomic regions that significantly associate with the resistance phenotype in an F_2 population segregating for dicamba-resistance (see Methods). Genes in these associated regions will be assessed for function annotations related to flavonol biosynthesis, regulation of the flavonol biosynthesis pathway, and auxin transport. This project will either add support for the current hypothesis by adding genome mapping evidence to the observed CHS and F3'H expression patterns identified by forward genetics approach or produce data to generate new hypotheses regarding the molecular mechanism of dicamba transport inhibition.

Table 1 – Real-Time PCR Primers. Primers used for qRT-PCR relative expression assays and for qPCR genomic copy number assays.

Transcript	ID	Sequence 5'->3'
Actin-1	Actin-1_F	GAGCATCCTGTCTTACTGACTG
	Actin-1_R	ATGAGAGAACGGCCTGAATG
ALS	ALS_F	ATGCAGACAATGTTGGATAC
	ALS_R	TCAACCATCGATACGAACAT
SEC5	SEC5_F	TATGGACTCAGACATGTATGG
	SEC5_R	CTGATTCCAATGTGACTGCG
CHS	TT4_10090_F	TTCAAAGGAACGCTGTGAAGG
	TT4_10090_R	CCAAATTGGGCCTAAAGGAAG
F3'H	TT7_1223/850_F	GGTTATGTGAAGAGAATGAAGG
	TT7_1223/850_R	CTGAACTTTCTGTACCACCGG
FLS	FLS_15979_F	AGTTAATGGAGGTGGAGAAGG
	FLS_15979_R	AGAAATCAAACGGACTAAGCG
WRKY23	WRKY23_6166_F	AACAGGAGCAGAATTTGCAGC
	WRKY23_6166_R	CCAATAACCATCATGGCTTCC

Table 2 – Dose Response Curve Variables. Parameter estimates of the 4-parameter nonlinear regression analysis of herbicide rates causing 50% growth reduction (GR_{50}) show 5× resistance to dicamba in 9425R compared to 7710S. Standard Error listed in parentheses.

Line	Slope	Lower Limit	Upper Limit	GR_{50}	GR_{50} R/S ratio
9425R	1.18 (0.24)	1.25 (4.86)	107.6 (4.9)	426.8 (79.86)	5.1
7710S	1.95 (0.37)	0.07 (2.31)	98.4 (2.97)	83.38 (9.42)	-

Table 3 – SNP Calls and Differential Expression: Auxin Receptors and Transporters.

Annotation	Transcriptome Locus	Non-Synonymous SNPs	Differential Expression from GLM terms		
			“Line”	“Treatment”	“Line*Treatment”
ABP1	N/A	N/A	N/A	N/A	N/A
TIR1	Locus_115	N/A	N/A	N/A	N/A
AFB3	Locus_536	N/A	N/A	N/A	N/A
	Locus_7918	N/A	N/A	N/A	N/A
AFB5	Locus_1445	N/A	N/A	N/A	N/A
SKP2A	Locus_6180	N/A	N/A	N/A	N/A
PIN3	Locus_2310	N/A	N/A	N/A	N/A
PIN4	Locus_28729	N/A	N/A	N/A	N/A
PIN5	Locus_19075	N/A	N/A	N/A	N/A
ABCB1	Locus_9522	N/A	N/A	N/A	N/A
ABCB19	Locus_14262	N/A	N/A	N/A	N/A
AUX1	Locus_3681	N/A	N/A	N/A	N/A
LAX2	Locus_875	N/A	N/A	N/A	N/A

Table 4 – F₂ Phenotypic Distribution. X² test for 3:1 inheritance of resistant to susceptible phenotype distribution in F₂ population confirms single-gene dominant inheritance of resistance phenotype.

	Resistant	Susceptible	X ²	p-value
Observed	130	50	0.74074	0.3894
Expected	(135)	(45)		

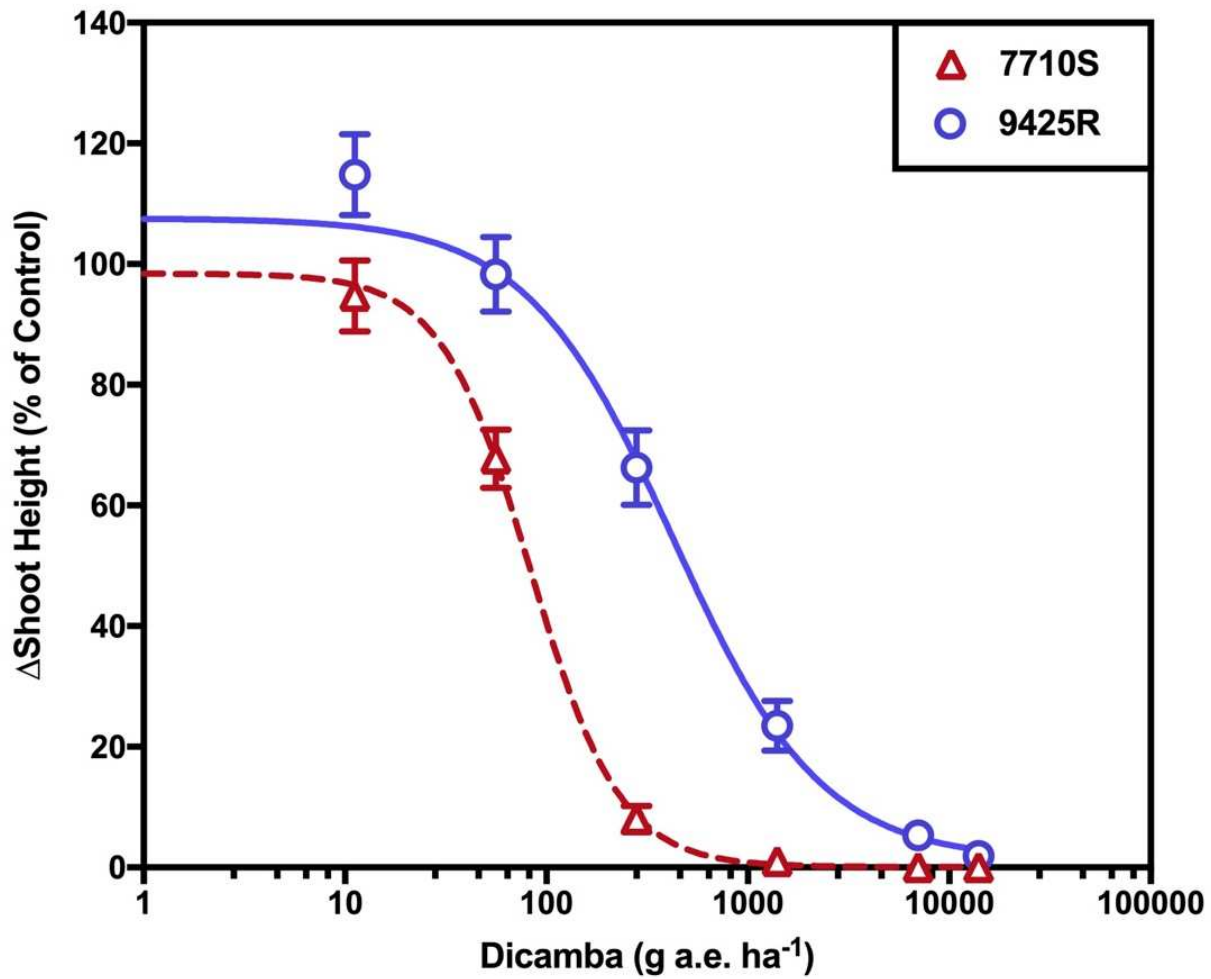


Figure 1 – Dicamba Dose Response Curves. 9425R is more resistant to dicamba treatment than 7710S. Each line was fit to a 4-parameter log-logistic curve. Bars represent standard error.

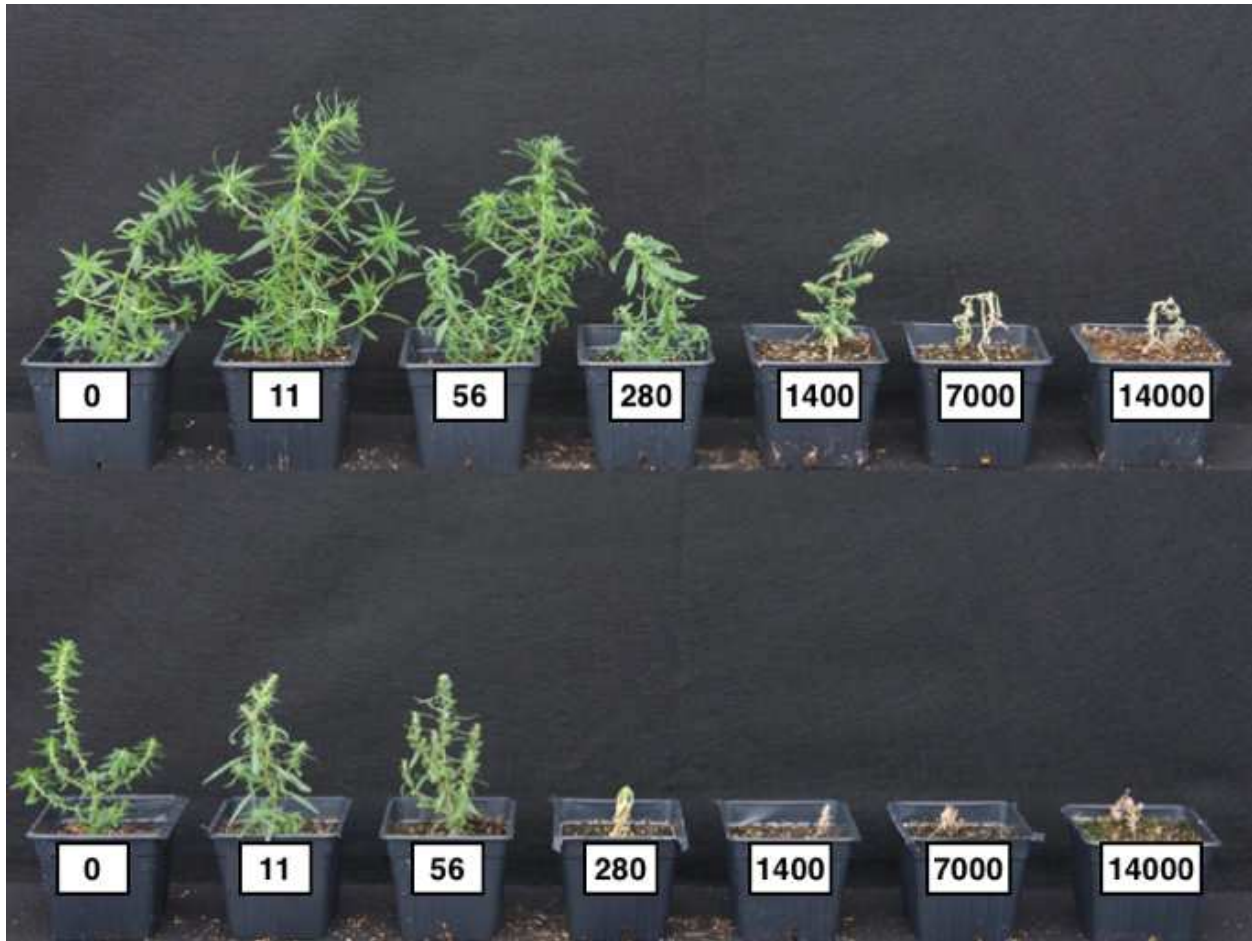


Figure 2 – Dicamba Dose Response Image. 9425R above shows greater resistance to dicamba than 7710S below. Dicamba treatments presented in g a.e. ha⁻¹.

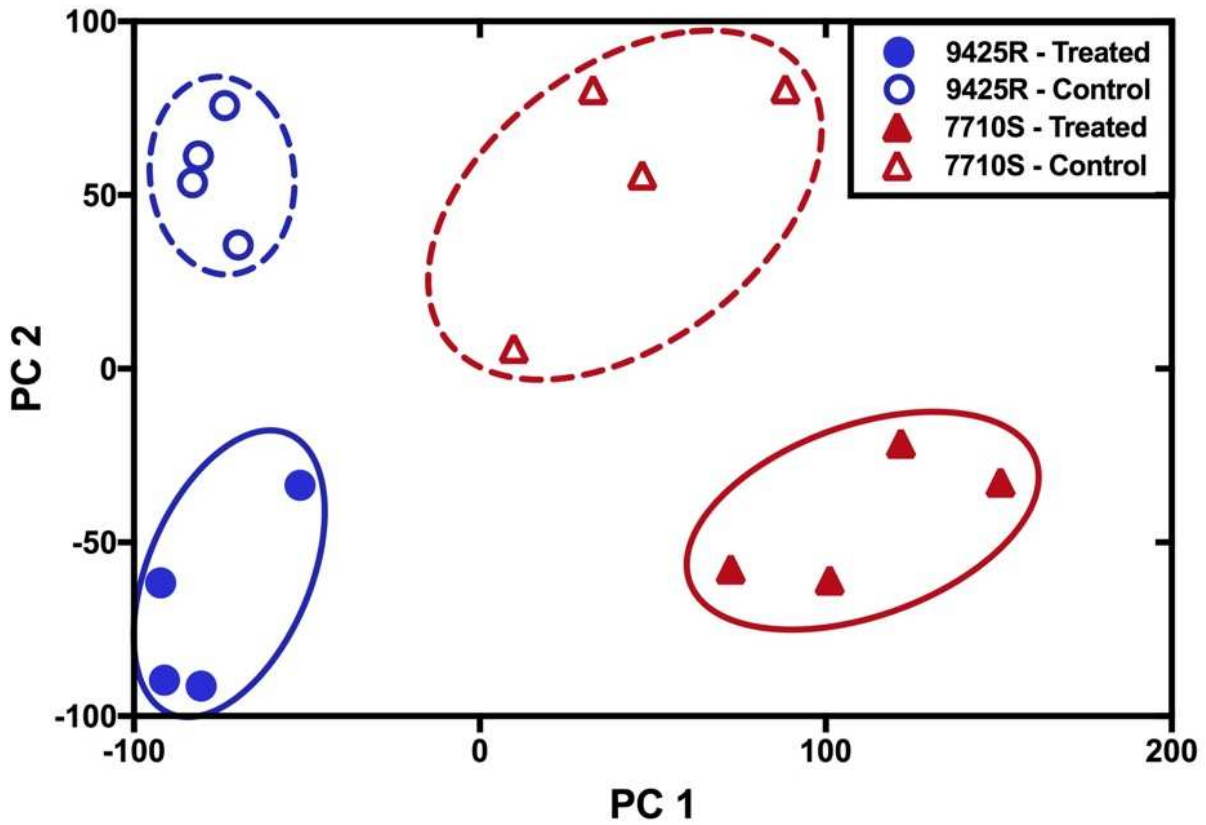


Figure 3 – RNA-seq Principle Components Analysis. Transcript-level expression shows primary differentiation of individuals by genetic background (PC 1) and secondarily by treatment (PC 2).

Figure 4 – GLM Terms: Venn Diagram. Genetic background ('Line') explains most of the significantly differentially expressed transcripts identified using the generalized linear model ($Y = \text{Line} + \text{Treatment} + \text{Line} * \text{Treatment}$). Numbers represent individual transcripts.

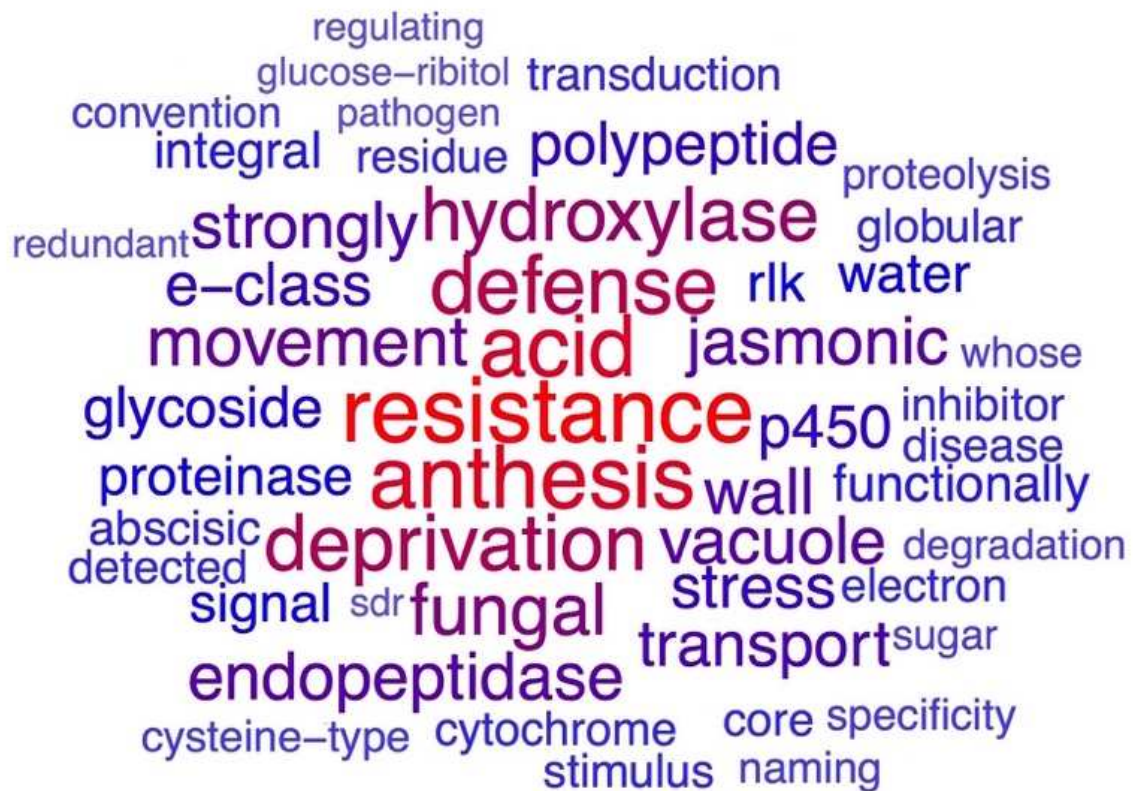


Figure 5 – Line*Treatment Genecloud. GeneCloud analysis shows significant transcripts identified for the generalized linear model term, “Line*Treatment” are enriched for resistance, defense, stress, and transport-related keywords.

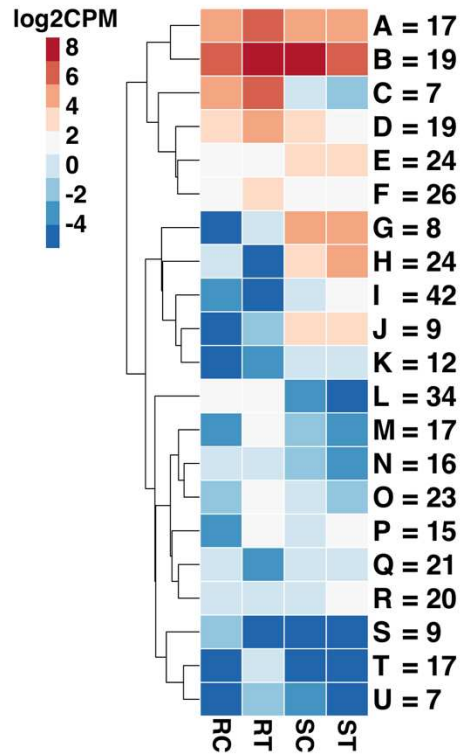


Figure 6 – Line*Treatment Heatmap. Clustered heatmap shows expression trends of all 386 significant contigs identified by the generalized linear model interaction term. Row names indicate the number of transcripts represented by each K-means cluster (“RC” = 9425R-Control, “RT” = 9425R-Treated, “SC” = 7710S-Control, “ST” = 7710S-Treated).

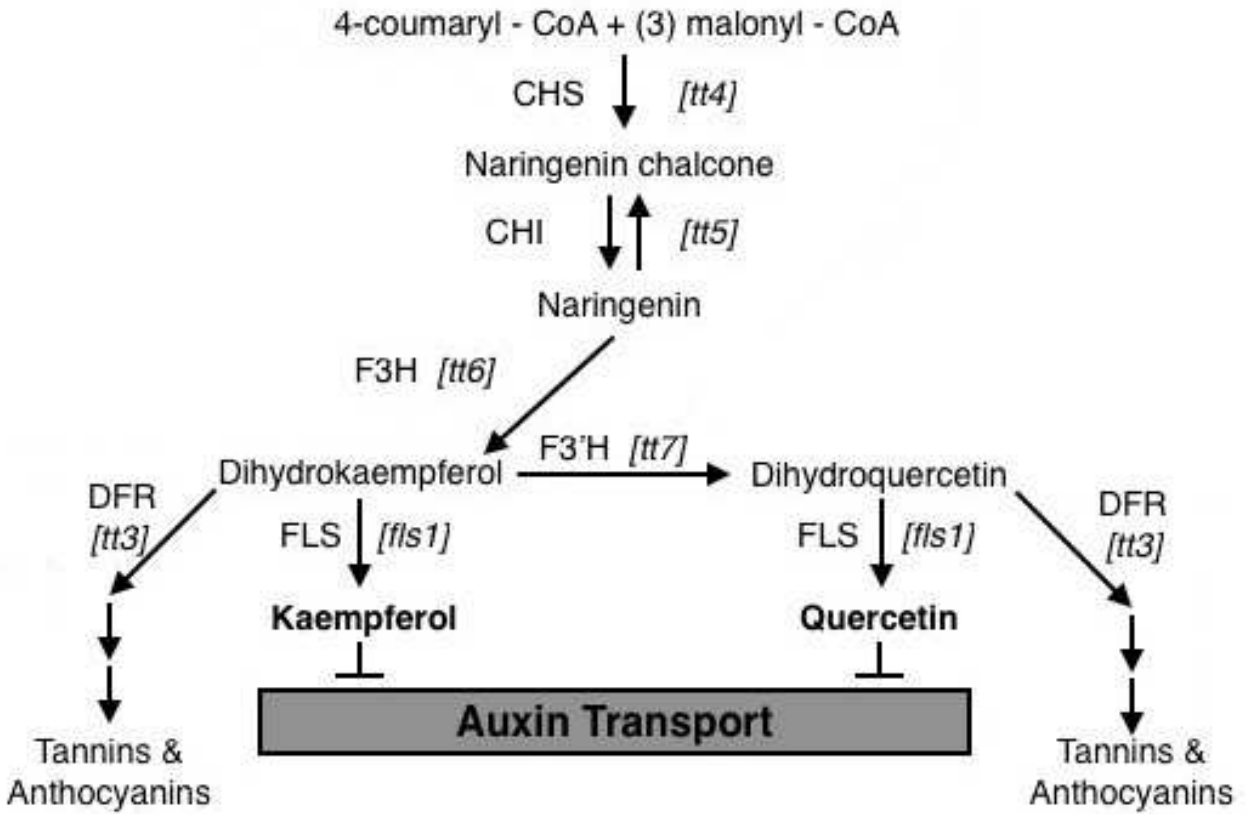


Figure 7 – Flavonol Biosynthesis Pathway in *Arabidopsis thaliana*. Image adapted from Murphy et al. (2000).

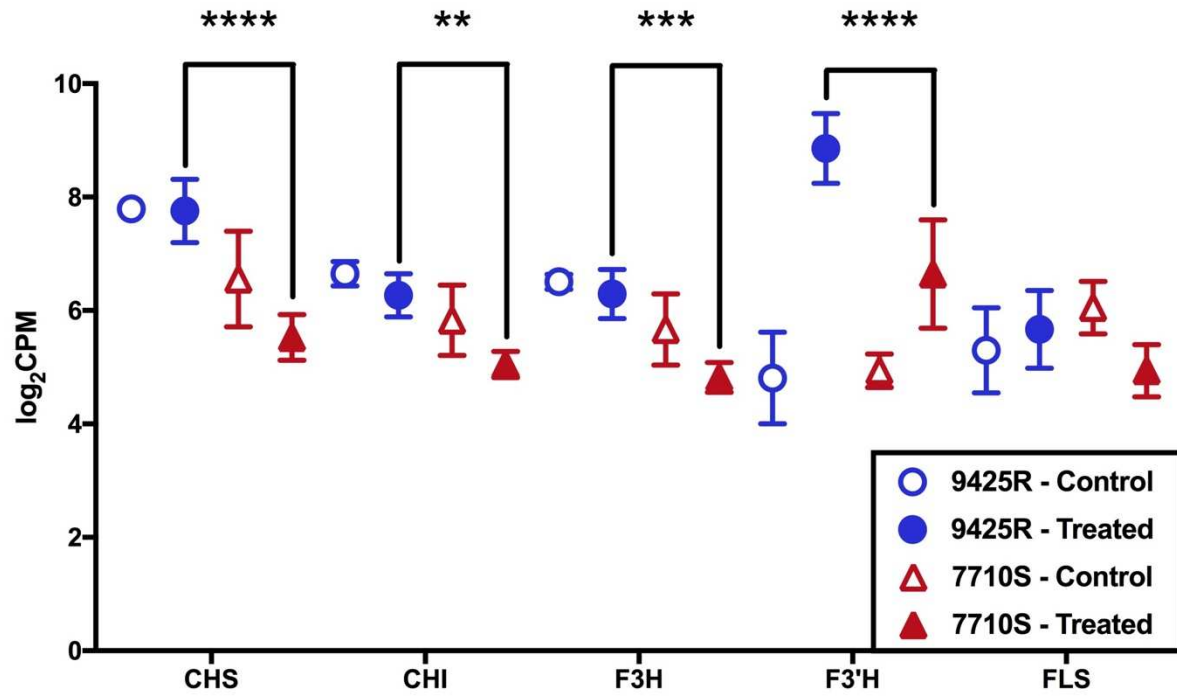


Figure 8 – Flavonol Biosynthesis: *in silico* Expression. RNA-seq expression data shows significant upregulation of flavonol biosynthesis in 9425R compared to 7710S.

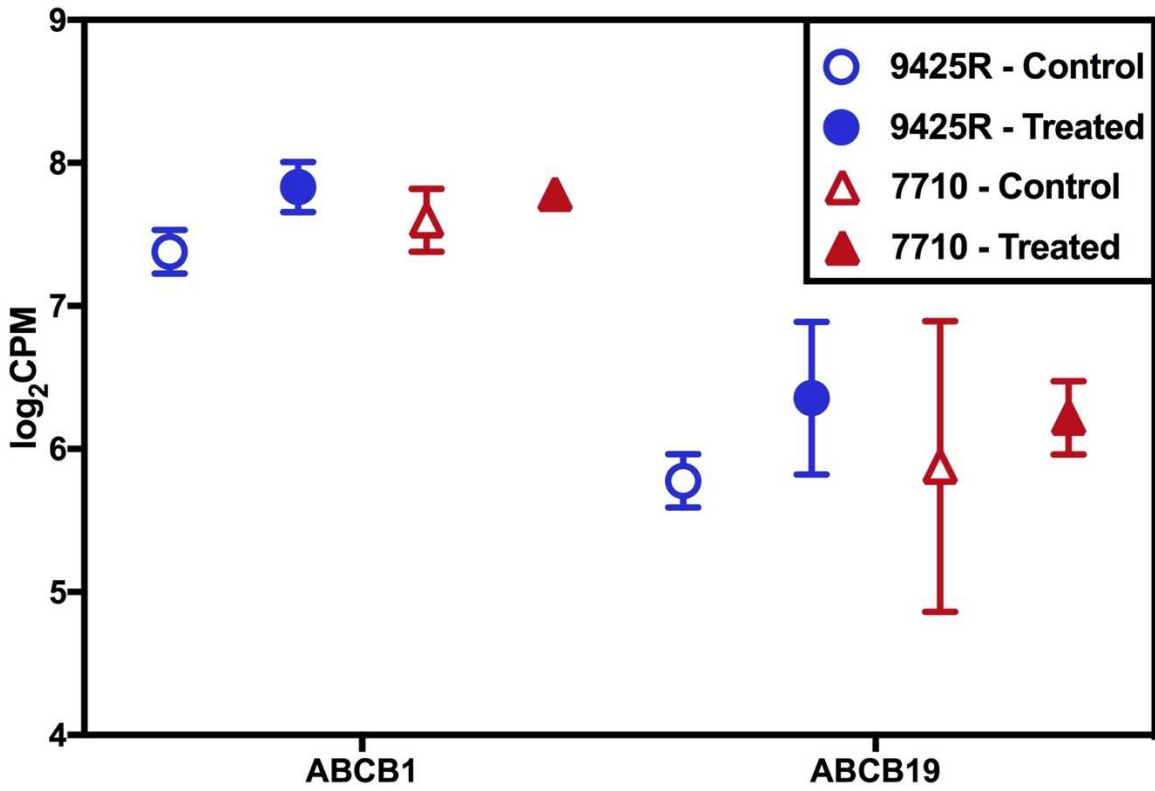


Figure 9 – ABCB Auxin Transporters: *in silico* Expression. No significant differences in expression were identified for ABCB transporters with activities related to auxin transport.

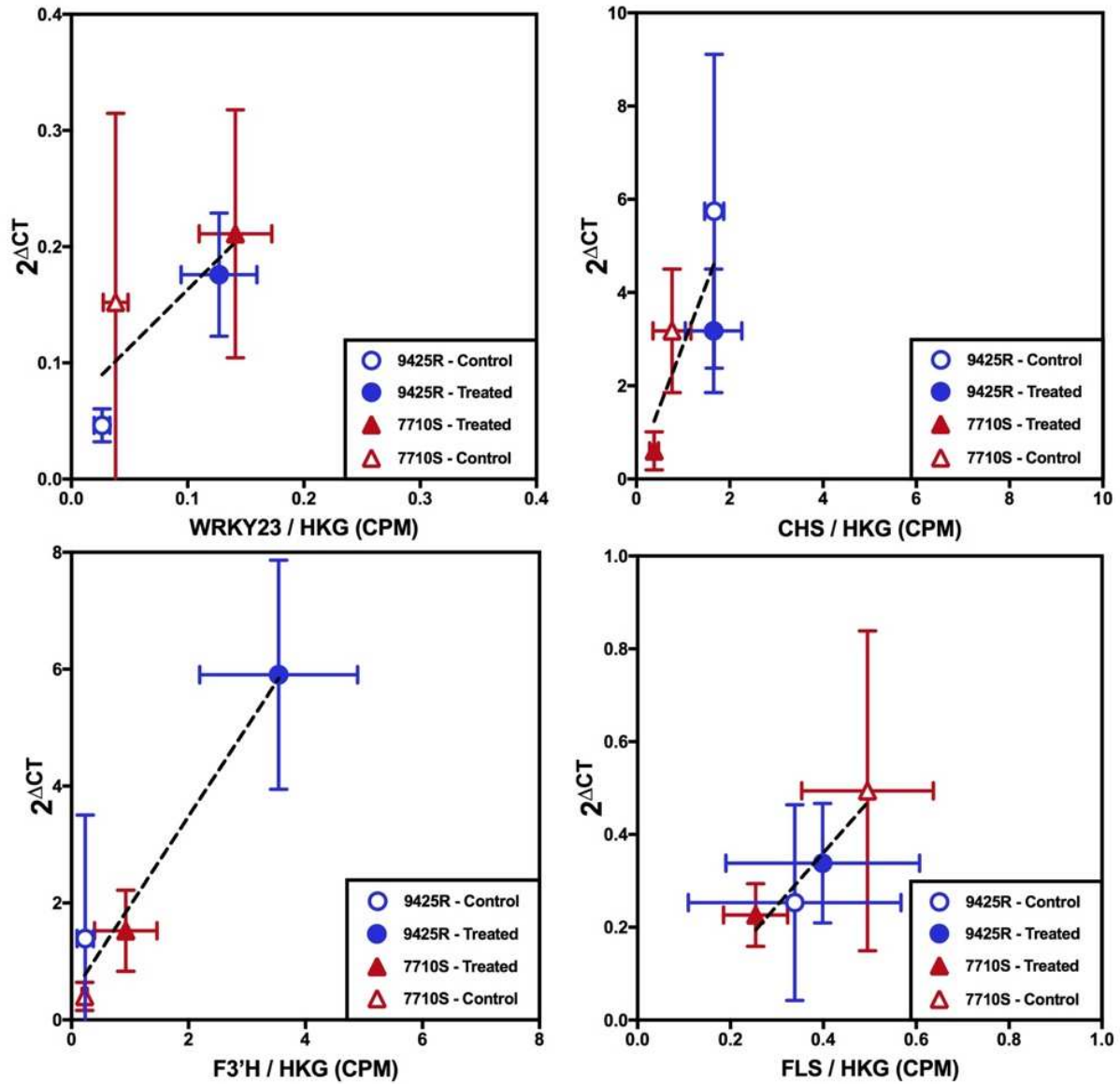


Figure 10 – qRT-PCR and *in silico* Expression Regression. qRT-PCR expression values correlate with *in silico* expression values from RNA-seq. The relative CPM of each contig compared the geometric mean of the three housekeeping genes (Actin-1, ALS, SEC5). Linear regression R^2 values: WRKY23=0.69, CHS=0.66, F3'H=0.97, FLS=0.92.

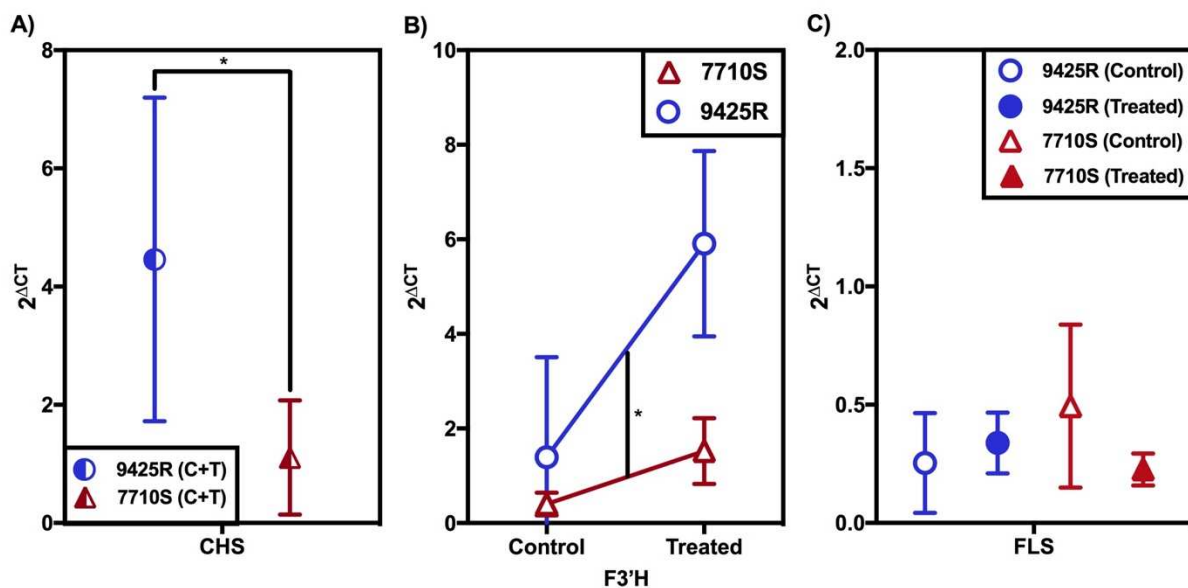


Figure 11 – qRT-PCR Validation of Flavonol Biosynthesis Expression. qRT-PCR validation of RNA-seq confirms A) effect of “line” on CHS expression, B) “line*treatment” effect of F3’H and C) no significant differences for FLS.

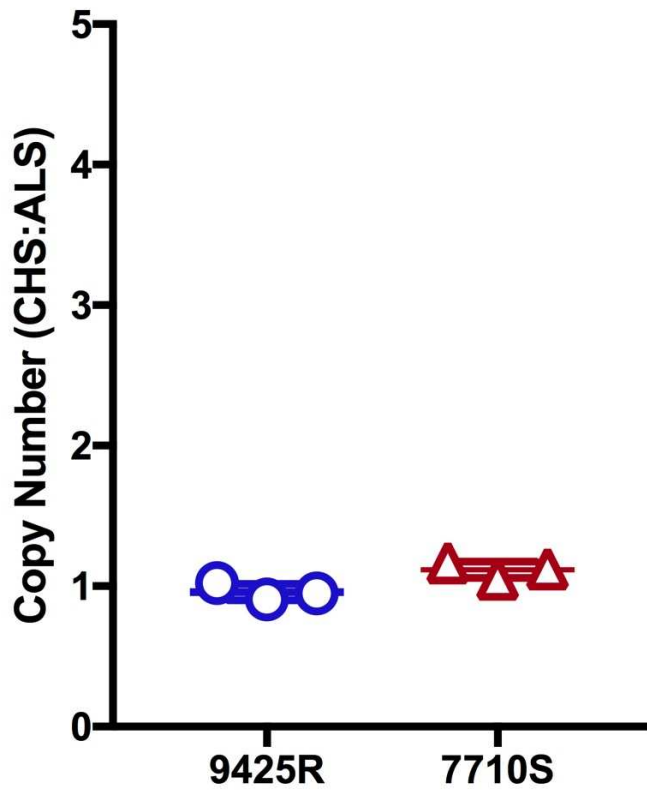


Figure 12 – CHS Genomic Copy Number. Genomic copy number analysis shows no difference in CHS:ALS relative copy number between of 0.96 for 9425R and 1.12 for 7710S (n=3, bars represent the mean and standard deviation).

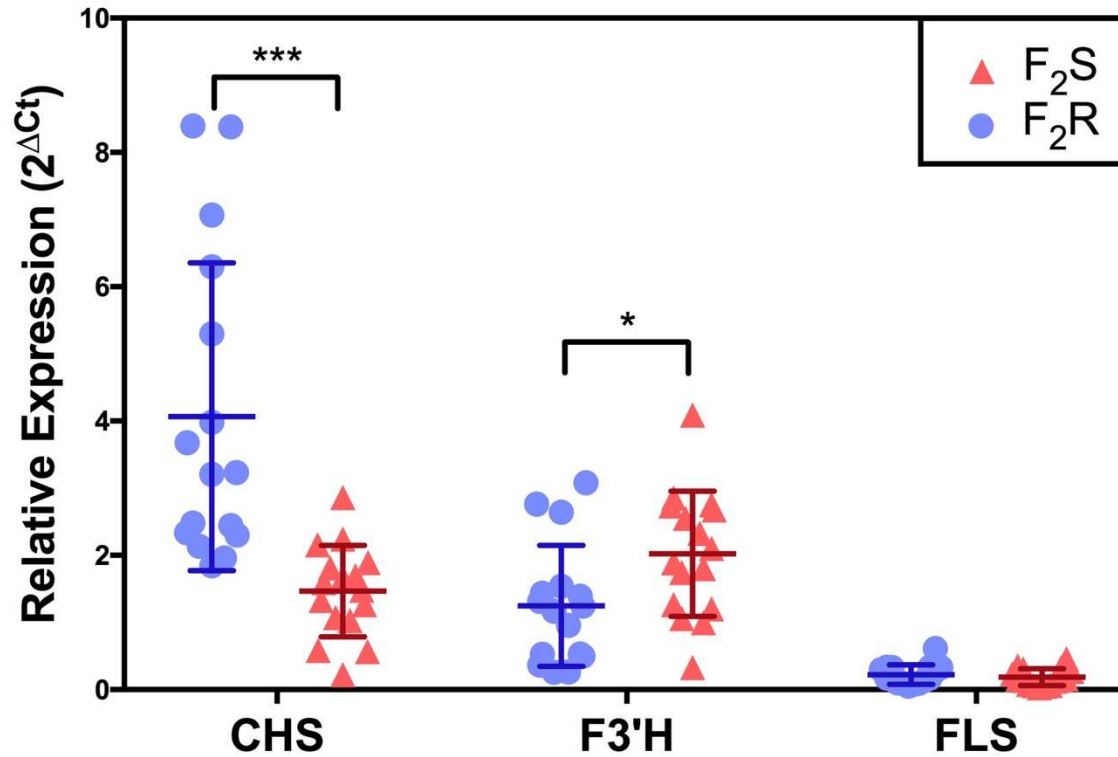


Figure 13 – Co-segregation of Flavonol Biosynthesis Expression Profile with Phenotype in F₂. The dicamba-resistant phenotype (F₂R) co-segregates in the F₂ population with the 9425R parental transcription pattern for CHS, measured with qRT-PCR; transcription level of F3'H was significantly different between F₂R and F₂S, but did not follow the 9425R parental transcription pattern. No significant expression difference detected in FLS. Measurements taken 12 hours after dicamba treatment (n=16).

REFERENCES

- Abel S, Theologis A** (1996) Early genes and auxin action. *Plant Physiol* **111**: 9–17
- Artimo P, Jonnalagedda M, Arnold K, Baratin D, Csardi G, De Castro E, Duvaud S, Flegel V, Fortier A, Gasteiger E, et al** (2012) ExPASy: SIB bioinformatics resource portal. *Nucleic Acids Res* **40**: 1–7
- Bailly A, Sovero V, Vincenzetti V, Santelia D, Bartnik D, Koenig BW, Mancuso S, Martinoia E, Geisler M** (2008) Modulation of P-glycoproteins by auxin transport inhibitors is mediated by interaction with immunophilins. *J Biol Chem* **283**: 21817–21826
- Bandyopadhyay A, Blakeslee JJ, Lee OR, Mravec J, Sauer M, Titapiwatanakun B, Makam SN, Bouchard R, Geisler M, Martinoia E, et al** (2007) Interactions of PIN and PGP auxin transport mechanisms. *Biochem Soc Trans* **35**: 137–41
- Bateman A, Martin MJ, O'Donovan C, Magrane M, Apweiler R, Alpi E, Antunes R, Arganiska J, Bely B, Bingley M, et al** (2015) UniProt: A hub for protein information. *Nucleic Acids Res* **43**: D204–D212
- Beckie HJ, Blackshaw RE, Hall LM, Johnson EN** (2016) Pollen- and Seed-Mediated Gene Flow in *Kochia* (*Kochia scoparia*). *Weed Sci* **64**: 624–633
- Behrens MR, Mutlu N, Chakraborty S, Dumitru R, Jiang WZ, LaVallee BJ, Herman PL, Clemente TE, Weeks DP** (2007) Dicamba resistance: enlarging and preserving biotechnology-based weed management strategies. *Science* (80-) **316**: 1185–1188
- Bell AR, Nalewaja JD, Schooler AB** (1972) Light period, temperature, and *kochia* flowering. *Weed Sci* 462–464
- Belles DS** (2004) The Genetics and Physiology of Dicamba Resistance in *Kochia* (*Kochia Scoparia* L. Schrad.). Colorado State University
- Benková E, Michniewicz M, Sauer M, Teichmann T, Seifertová D, Jürgens G, Friml J** (2003) Local, Efflux-Dependent Auxin Gradients as a Common Module for Plant Organ Formation. *Cell* **115**: 591–602
- Berardini TZ, Reiser L, Li D, Mezheritsky Y, Muller R, Strait E, Huala E** (2015) The arabidopsis information resource: Making and mining the “gold standard” annotated reference plant genome. *Genesis* **53**: 474–485
- Blakeslee JJ, Bandyopadhyay A, Lee OR, Mravec J, Titapiwatanakun B, Makam SN, Sauer M, Cheng Y, Bouchard R, Adamec J, et al** (2007) Interactions among PIN-FORMED and P-Glycoprotein Auxin Transporters in *Arabidopsis*. *Plant Cell* **19**: 131–147
- Blilou I, Xu J, Wildwater M, Willemsen V, Paponov I, Friml J, Heidstra R, Aida M, Palme K, Scheres B** (2005) The PIN auxin efflux facilitator network controls growth and patterning in *Arabidopsis* roots. *Nature* **433**: 39–44
- Brock G, Pihur V, Datta SS** (2008) cIValid : An R Package for Cluster Validation. *J Stat Softw* **25**: 1–28
- Brown DE, Rashotte AM, Murphy AS, Normanly J, Tague BW, Peer WA, Taiz L, Muday GK** (2001) Flavonoids act as negative regulators of auxin transport in vivo in *Arabidopsis*. *Plant Physiol* **126**: 524–535
- Buer CS, Muday GK** (2004) The transparent testa4 Mutation Prevents Flavonoid Synthesis and Alters Auxin Transport and the Response of *Arabidopsis* Roots to Gravity and Light. *Plant Cell* **15**: 1191–1205

- Camacho C, Coulouris G, Avagyan V, Ma N, Papadopoulos J, Bealer K, Madden TL** (2009) BLAST plus: architecture and applications. *BMC Bioinformatics* **10**: 1
- Cao M, Sato SJ, Behrens M, Jiang WZ, Clemente TE, Weeks DP** (2011) Genetic engineering of maize (*Zea mays*) for high-level tolerance to treatment with the herbicide dicamba. *J Agric Food Chem* **59**: 5830–5834
- Christoffoleti PJ, de Figueiredo MRA, Peres LEP, Nissen S, Gaines T** (2015) Auxinic herbicides, mechanisms of action, and weed resistance: A look into recent plant science advances. *Sci Agric* **72**: 356–362
- Collins RP, Jones MB** (1986) The influence of climatic factors on the distribution of C4 species in Europe. *Vegetatio* **64**: 121–129
- Cranston HJ, Kern AJ, Hackett JL, Miller EK, Maxwell BD, Dyer WE** (2001) Dicamba resistance in kochia. *Weed Sci* **49**: 164–170
- Dill GM, CaJacob CA, Padgett SR** (2008) Glyphosate-resistant crops: adoption, use and future considerations. *Pest Manag Sci* **64**: 326–331
- Evetts LL, Burnside OC** (1972) Germination and seedling development of common milkweed and other species. *Weed Sci* **20**: 371–378
- Friesen LF, Beckie HJ, Warwick SI, Van Acker RC** (2009) The biology of Canadian weeds. 138. *Kochia scoparia* (L.) Schrad. *Can J Plant Sci* **89**: 141–167
- Friml J, Wiśniewska J, Benková E, Mendgen K, Palme K** (2002) Lateral relocation of auxin efflux regulator PIN3 mediates tropism in *Arabidopsis*. *Nature* **415**: 806–809
- Gaines TA, Zhang W, Wang D, Bukun B, Chisholm ST, Shaner DL, Nissen SJ, Patzoldt WL, Tranel PJ, Culpepper AS, et al** (2010) Gene amplification confers glyphosate resistance in *Amaranthus palmeri*. *Proc Natl Acad Sci* **107**: 1029–1034
- Gälweiler L, Guan C, Müller A, Wisman E, Mendgen K, Yephremov A, Palme K** (1998) Regulation of Polar Auxin Transport by AtPIN1 in *Arabidopsis* Vascular Tissue. *Science* (80-) **282**: 2226–2230
- Geisler M, Blakeslee JJ, Bouchard R, Lee OR, Vincenzetti V, Bandyopadhyay A, Titapiwatanakun B, Peer WA, Bailly A, Richards EL, et al** (2005) Cellular efflux of auxin catalyzed by the *Arabidopsis* MDR/PGP transporter AtPGP1. *Plant J* **44**: 179–194
- Geisler M, Murphy AS** (2006) The ABC of auxin transport: the role of p-glycoproteins in plant development. *FEBS Lett* **580**: 1094–1102
- Gleason C, Foley RC, Singh KB** (2011) Mutant analysis in *Arabidopsis* provides insight into the molecular mode of action of the auxinic herbicide dicamba. *PLoS One* **6**: e17245
- Goldsmith MHM** (1977) The Polar Transport of Auxin. *Annu Rev Plant Physiol* **28**: 439–478
- Goss GA, Dyer WE** (2003) Physiological characterization of auxinic herbicide-resistant biotypes of kochia (*Kochia scoparia*). *Weed Sci* **51**: 839–844
- Gray WM, Kepinski S, Rouse D, Leyser O, Estelle M** (2001) Auxin regulates SCFTIR1-dependent degradation of AUX/IAA proteins. *Nature* **414**: 271–276
- Grieneisen VA, Xu J, Marée AFM, Hogeweg P, Scheres B** (2007) Auxin transport is sufficient to generate a maximum and gradient guiding root growth. *Nature* **449**: 1008–1013
- Grones P, Chen X, Simon S, Kaufmann WA, De Rycke R, Nodzynski T, Zazimalova E, Friml J** (2015) Auxin-binding pocket of ABP1 is crucial for its gain-of-function cellular and developmental roles. *J Exp Bot* **66**: 5055–5065
- Grossmann K** (2010) Auxin herbicides: current status of mechanism and mode of action. *Pest Manag Sci* **66**: 113–120
- Grunewald W, Smet I De, Lewis DR, Löffke C, Jansen L, Goeminne G, Bosschea R Vanden,**

- Karimi M, Rybela B De, Vanholmea B, et al** (2011) Transcription factor WRKY23 assists auxin distribution patterns during Arabidopsis root development through local control on flavonol biosynthesis. *Proc Natl Acad Sci* **109**: 1554–1559
- Hall JC, Alam SMM, Murr DP** (1993) Ethylene biosynthesis following foliar application of picloram to biotypes of wild mustard (*Sinapis arvensis* L.) susceptible or resistant to auxinic herbicides. *Pestic Biochem Physiol* **47**: 36–43
- Heap I** (2016) The International Survey of Herbicide Resistant Weeds. www.weedscience.org
- Heap IM, Morrison IN** (1992) Resistance to auxin-type herbicides in wild mustard (*Sinapis arvensis* L.). *Proc. Weed Sci. Soc. Am.* pp 32–55
- Henrichs S, Wang B, Fukao Y, Zhu J, Charrier L, Bailly A, Oehring SC, Linnert M, Weiwad M, Endler A, et al** (2012) Regulation of ABCB1/PGP1-catalysed auxin transport by linker phosphorylation. *EMBO J* **31**: 2965–80
- Herman PL, Behrens M, Chakraborty S, Chrastil BM, Barycki J, Weeks DP** (2005) A three-component dicamba O-demethylase from *Pseudomonas maltophilia*, strain DI-6: gene isolation, characterization, and heterologous expression. *J Biol Chem* **280**: 24759–24767
- Jacobs M, Rubery PH** (1988) Naturally Occurring Auxin Transport Regulators. *Science* (80-) **241**: 346–349
- Jasieniuk M, Morrison IN, Brule-Babel AL** (1995) Inheritance of dicamba resistance in Wild Mustard (*Brassica Kaber*). *Weed Sci* **43**: 192–195
- Jurado S, Abraham Z, Manzano C, López-Torrejón G, Pacios LF, Del Pozo JC** (2010) The Arabidopsis cell cycle F-box protein SKP2A binds to auxin. *Plant Cell* **22**: 3891–904
- Kamphausen T, Fanghänel J, Neumann D, Schulz B, Rahfeld JU** (2002) Characterization of Arabidopsis thaliana AtFKBP42 that is membrane-bound and interacts with Hsp90. *Plant J* **32**: 263–276
- Kang J, Park J, Choi H, Burla B, Kretschmar T, Lee Y, Martinoia E** (2011) Plant ABC Transporters. *Arabidopsis Book* **9**: e0153
- Keilig K, Ludwig-Mueller J** (2009) Effect of flavonoids on heavy metal tolerance in Arabidopsis thaliana seedlings. *Bot Stud* **50**: 311–318
- Kelley KB, Riechers DE** (2007) Recent developments in auxin biology and new opportunities for auxinic herbicide research. *Pestic Biochem Physiol* **89**: 1–11
- Kern A, Chaverra M, Cranston H, Dyer W** (2005) Dicamba-Responsive Genes in Herbicide-Resistant and Susceptible Biotypes of Kochia (*Kochia scoparia*). *Weed Sci* **53**: 139–145
- Kleine-Vehn J, Ding Z, Jones AR, Tasaka M, Morita MT, Friml J** (2010) Gravity-induced PIN transcytosis for polarization of auxin fluxes in gravity-sensing root cells. *Proc Natl Acad Sci* **107**: 22344–22349
- Knezevic SZ, Streibig JC, Ritz C** (2007) Utilizing R Software Package for Dose-Response Studies: The Concept and Data Analysis. *Weed Technol* **21**: 840–848
- Kolde R** (2015) pheatmap: Pretty Heatmaps. R Package Version 1.0.8. 1–7
- Krouk G, Carré C, Fizames C, Gojon A, Ruffel S, Lacombe B** (2015) GeneCloud reveals semantic enrichment in lists of gene descriptions. *Mol Plant* **8**: 971–973
- Kuhn BM, Errafi S, Bucher R, Dobrev P, Geisler M, Bigler L, Zazmalov E, Ringli C** (2016) 7-Rhamnosylated Flavonols Modulate Homeostasis of the Plant Hormone Auxin and Affect Plant Development. *J Biol Chem* **291**: 5385–5395
- Kuhn BM, Geisler M, Bigler L, Ringli C** (2011) Flavonols accumulate asymmetrically and affect auxin transport in Arabidopsis. *Plant Physiol* **156**: 585–595

- Langmead B, Salzberg SL** (2012) Fast gapped-read alignment with Bowtie 2. *Nat Methods* **9**: 357–359
- Li H, Handsaker B, Wysoker A, Fennell T, Ruan J, Homer N, Marth G, Abecasis G, Durbin R** (2009) The Sequence Alignment/Map format and SAMtools. *Bioinformatics* **25**: 2078–2079
- Livak KJ, Schmittgen TD** (2001) Analysis of relative gene expression data using real-time quantitative PCR and the $2(-\Delta\Delta C(t))$ method. *Methods* **25**: 402–408
- Mengitsu LW, Messersmith CG** (2002) Genetic diversity of Kochia. *Weed Sci* **50**: 498–503
- Mithila J, Hall JC** (2005) Comparison of ABP1 over-expressing Arabidopsis and under-expressing tobacco with an auxinic herbicide-resistant wild mustard (*Brassica Kaber*) biotype. *Plant Sci* **169**: 21–28
- Morris ME, Zhang S** (2006) Flavonoid-drug interactions: effects of flavonoids on ABC transporters. *Life Sci* **78**: 2116–2130
- Murphy A, Peer WA, Taiz L** (2000) Regulation of auxin transport by aminopeptidases and endogenous flavonoids. *Planta* **211**: 315–324
- Nakabayashi R, Yonekura-Sakakibara K, Urano K, Suzuki M, Yamada Y, Nishizawa T, Matsuda F, Kojima M, Sakakibara H, Shinozaki K, et al** (2014) Enhancement of oxidative and drought tolerance in Arabidopsis by overaccumulation of antioxidant flavonoids. *Plant J* **77**: 367–379
- Nussbaum ES, Wiese AF, Crutchfield DE, Chenault EW, Lavake D** (1985) The Effects of Temperature and Rainfall on Emergence and Growth of Eight Weeds. *Weed Sci* **33**: 165–170
- Peer WA, Murphy AS** (2007) Flavonoids and auxin transport: modulators or regulators? *Trends Plant Sci* **12**: 556–563
- Peniuk MG, Romano ML, Hall JC** (1993) Physiological investigations into the resistance of a wild mustard (*Sinapis arvensis* L.) biotype to auxinic herbicides. *Weed Res* **33**: 431–440
- Pfaffl MW, Tichopad A, Prgomet C, Neuvians TP** (2004) Determination of stable housekeeping genes, differentially regulated target genes and sample integrity: BestKeeper – Excel-based tool using pair-wise correlations. *Biotechnol Lett* **26**: 509–515
- Di Pietro A, Conseil G, Pérez-Victoria JM, Dayan G, Baubichon-Cortay H, Tromprier D, Steinfels E, Jault JM, De Wet H, Maitrejean M, et al** (2002) Modulation by flavonoids of cell multidrug resistance mediated by P-glycoprotein and related ABC transporters. *Cell Mol Life Sci* **59**: 307–322
- Powles SB** (2008) Evolved glyphosate-resistant weeds around the world: lessons to be learnt. *Pest Manag Sci* **64**: 360–365
- Powles SB, Lorraine-colwill DF, Dellow JJ, Preston C** (1998) Evolved Resistance to Glyphosate in Rigid Ryegrass (*Lolium rigidum*) in Australia. *Weed Sci* **46**: 604–607
- del Pozo JC, Diaz-Trivino S, Cisneros N, Gutierrez C** (2006) The balance between cell division and endoreplication depends on E2FC-DPB, transcription factors regulated by the ubiquitin-SCFSKP2A pathway in Arabidopsis. *Plant Cell* **18**: 2224–2235
- Preston C, Belles DS, Westra PH, Nissen SJ, Ward SM** (2009) Inheritance of resistance to the auxinic herbicide dicamba in kochia (*Kochia scoparia*). *Weed Sci* **57**: 43–47
- Pyankov VI, Artyusheva EG, Edwards GE** (1999) Formation of C4 syndrome in leaves and cotyledons of *Kochia scoparia* and *Salsola collina* (Chenopodiaceae). *Russ J Plant Physiol* **46**: 452–466

- Rice P, Longden I, Bleasby A** (2000) EMBOSS: The European Molecular Biology Open Software Suite. *Trends Genet* **16**: 276–277
- Ringli C, Bigler L, Kuhn BM, Leiber R-M, Diet A, Santelia D, Frey B, Pollmann S, Klein M** (2008) The modified flavonol glycosylation profile in the Arabidopsis rol1 mutants results in alterations in plant growth and cell shape formation. *Plant Cell* **20**: 1470–81
- Ritz C, Streibig JC** (2005) Bioassay Analysis using R. *J Stat Softw* **12**: 1–22
- Robert S, Kleine-Vehn J, Barbez E, Sauer M, Paciorek T, Baster P, Vanneste S, Zhang J, Simon S, Covanova M, et al** (2010) ABP1 mediates auxin inhibition of clathrin-dependent endocytosis in Arabidopsis. *Cell* **143**: 111–121
- Robinson MD, McCarthy DJ, Smyth GK** (2009) edgeR: A Bioconductor package for differential expression analysis of digital gene expression data. *Bioinformatics* **26**: 139–140
- Rodriguez-Serrano M, Pazmino DM, Sparkes I, Rochetti A, Hawes C, Romero-Puertas MC, Sandalio LM** (2014) 2,4-Dichlorophenoxyacetic acid promotes S-nitrosylation and oxidation of actin affecting cytoskeleton and peroxisomal dynamics. *J Exp Bot* **65**: 4783–4793
- Ruiz Rosquete M, Barbez E, Kleine-Vehn J** (2012) Cellular auxin homeostasis: gatekeeping is housekeeping. *Mol Plant* **5**: 772–786
- Sabatini S, Beis D, Wolkenfelt H, Murfett J, Guilfoyle T, Malamy J, Benfey P, Leyser O, Bechtold N, Weisbeek P, et al** (1999) An auxin-dependent distal organizer of pattern and polarity in the Arabidopsis root. *Cell* **99**: 463–472
- Salehin M, Bagchi R, Estelle M** (2015) SCFTIR1/AFB-based auxin perception: mechanism and role in plant growth and development. *Plant Cell* **27**: 9–19
- Sauer M, Robert S, Kleine-Vehn J** (2013) Auxin: simply complicated. *J Exp Bot* **64**: 2565–2577
- Schmittgen TD, Livak KJ** (2008) Analyzing real-time PCR data by the comparative CT method. *Nat Protoc* **3**: 1101–1108
- Schwinghamer TD, Van Acker RC** (2008) Emergence Timing and Persistence of Kochia (*Kochia Scoparia*). *Weed Sci* **56**: 37–41
- Sievers F, Wilm A, Dineen D, Gibson TJ, Karplus K, Li W, Lopez R, McWilliam H, Remmert M, Söding J, et al** (2011) Fast, scalable generation of high-quality protein multiple sequence alignments using Clustal Omega. *Mol Syst Biol* **7**: 539
- Simon S, Skúpa P, Viaene T, Zwiewka M, Tejos R, Klíma P, Čarná M, Rolčík J, De Rycke R, Moreno I, et al** (2016) PIN6 auxin transporter at endoplasmic reticulum and plasma membrane mediates auxin homeostasis and organogenesis in Arabidopsis. *New Phytol* **211**: 65–74
- Sterling T, Hall JC** (1997) *Herbicide Activity: Toxicology, Biochemistry and Molecular Biology*. IOS Press, Amsterdam
- Swarup R, Péret B** (2012) AUX/LAX family of auxin influx carriers-an overview. *Front Plant Sci* **3**: 225
- Team** (2016) R: A language and environment for statistical computing. R Found. Stat. Comput. Vienna, Austria
- Walsh TA, Neal R, Merlo AO, Honma M, Hicks GR, Wolff K, Matsumura W, Davies JP** (2006) Mutations in an auxin receptor homolog AFB5 and in SGT1b confer resistance to synthetic picolinate auxins and not to 2,4-dichlorophenoxyacetic acid or indole-3-acetic acid in Arabidopsis. *Plant Physiol* **142**: 542–552

- Wang XZ, Li B, Herman PL, Weeks DP** (1997) A three-component enzyme system catalyzes the O demethylation of the herbicide dicamba in *Pseudomonas maltophilia* DI-6. *Appl Environ Microbiol* **63**: 1623–1626
- Wang Y, Deshpande S, Hall JC** (2001) Calcium may mediate auxinic herbicide resistance in wild mustard. *Weed Sci* **49**: 2–7
- Wiersma AT, Gaines T a., Preston C, Hamilton JP, Giacomini D, Robin Buell C, Leach JE, Westra P** (2015) Gene amplification of 5-enol-pyruvylshikimate-3-phosphate synthase in glyphosate-resistant *Kochia scoparia*. *Planta* **241**: 463–474
- Wiese AF, Vandiver CW** (1970) Soil moisture effects on competitive ability of weeds. *Weed Sci* **18**: 518–519
- Wright TR, Shan G, Walsh TA, Lira JM, Cui C, Song P, Zhuang M, Arnold NL, Lin G, Yau K** (2010) Robust crop resistance to broadleaf and grass herbicides provided by aryloxyalkanoate dioxygenase transgenes. *Proc Natl Acad Sci* **107**: 20240–20245
- Wu G, Otegui MS, Spalding EP** (2010) The ER-localized TWD1 immunophilin is necessary for localization of multidrug resistance-like proteins required for polar auxin transport in *Arabidopsis* roots. *Plant Cell* **22**: 3295–3304
- Wu HM, Hazak O, Cheung AY, Yalovsky S** (2011) RAC/ROP GTPases and auxin signaling. *Plant Cell* **23**: 1208–1218
- Xu T, Dai N, Chen J, Nagawa S, Cao M, Li H, Zhou Z, Chen X, De Rycke R, Rakusová H** (2014) Cell surface ABP1-TMK auxin-sensing complex activates ROP GTPase signaling. *Science* (80-) **343**: 1025–1028
- Yin R, Han K, Heller W, Albert A, Dobrev PI, Zazimalova E, Schaffner AR** (2014) Kaempferol 3-O-rhamnoside-7-O-rhamnoside is an endogenous flavonol inhibitor of polar auxin transport in *Arabidopsis* shoots. *New Phytol* **201**: 466–475
- Zazimalova E, Murphy AS, Yang H, Hoyerova K, Hosek P** (2010) Auxin transporters--why so many? *Cold Spring Harb Perspect Biol* **2**: a001552
- Zhao J, Dixon RA** (2010) The “ins” and “outs” of flavonoid transport. *Trends Plant Sci* **15**: 72–80

APPENDIX: TWD1 GENOTYPING

INTRODUCTION

Role of TWD1 in Auxin Transport

The roles of ABCB transporters in auxin transport and plant development have been well described, but they are not able function as individual proteins. TWISTED DWARF 1 (TWD1) has been identified as a required partner for ABCB transporters to properly transport endogenous auxins. Analysis of *A. thaliana* mutants has demonstrated overlapping phenotypes between *twd1* knockouts and ABCB transporter knockouts caused by mis-regulation of auxin transport (Kamphausen et al., 2002; Bailly et al., 2008; Wu et al., 2010; Henrichs et al., 2012). Therefore, nonsense mutations coding for premature stop codons or non-synonymous mutations causing conformational changes in TWD1 proteins could disrupt auxin transport, potentially conferring a dicamba-resistant phenotype.

METHODS

TWD1 Genotyping

Consensus sequences for both 7710S and 9425R were produced using RNA-seq alignment data from all eight individuals of each line. The SAMtools function ‘mpileup’ (Li et al., 2009) extracted summary information from all eight alignment files per line, a call for each base was made using the BCFutils function ‘call’, and VCFutils was implemented to convert the data to a fastq file. In addition, putative peptide sequences were determined from fastq data files for TWD1 by extracting the amino acid sequence of the longest open reading frame for each line as determined using the ExPASy Translate tool (Artimo et al., 2012).

Putative peptide sequences of the consensus cDNA sequences generated for the TWD1 transcript from 7710S, 9425R, and *Arabidopsis thaliana* Col-0 (Berardini et al., 2015) were aligned using Clustal Omega (Sievers et al., 2011) (Figure 14, Figure 15) with default parameters. A non-synonymous mutation was identified in TWD1 between 7710S and 9425R, producing an S262G substitution. This codon change entails a switch from an amino acid with a polar R-group capable of hydrogen bonding to an amino acid with a single hydrogen R-group. Notably, this change eliminates the capacity for hydrogen bonding at amino acid 262, greatly reduces the size of the amino acid, and could produce conformational changes in the protein structure.

S262G KASP Assay

A KASP assay was designed to genotype *K. scoparia* individuals at the position of amino acid 262 in the TWD1 locus. Primers were designed from TWD1 genomic sequence data (unpublished data) (Table 5). Genomic DNA was extracted from 24 F₂ individuals identified as resistant (n=12) and susceptible (n=12) from the forward genetics screen (see Chapter 2: Methods) using the CTAB method. Genomic DNA from each individual was diluted to 5 ng/μL. The primer mixture was made containing primers Ks_TWD1_For_FAM, Ks_TWD1_For_FAM, and Ks_TWD1_Rev at final concentrations of 12 μM, 12 μM, and 30μM respectively, diluted in nuclease-free water. A 2× master mix was produced with 432 μL 2× KASP Master Mix (LGC) and 11.88 μL primer mixture. KASP reactions of 8 μL: 4 μL master mix and 4 μL genomic DNA at 5 ng/μL were run with the following cycling protocol: 94°C for 15 min; followed by 10 cycles of 94°C for 20 sec, 61-55°C for 60 Sec (0.6°C touchdown per cycle); followed by 25 cycles of 94°C for 20 sec, and 55°C for 60 sec. HEX and FAM fluorescence was quantified after

cycle number 25 and calls were made using the Bio-Rad CFX-Connect Software. Samples from lines 7710S and 9425R were used as positive controls for TWD1 locus 572 alleles C (FAM primer) and T (HEX primer), respectively. Synthetic heterozygous positive controls were generated with 50:50 mixtures of genomic DNA from 7710S and 9425R. Reactions with 4 μ L nuclease-free water in place of DNA template were used as negative controls.

RESULTS AND DISCUSSION

Genotype calls for F₂R and F₂S individuals did not co-segregate with the predicted grandparental genotypes of 9425R and 7710S (Figure 16). This lack of correlation suggests that the observed mutation between 9425R and 7710S does not confer the differential dicamba response phenotypes.

Table 5 – TWD1 KASP Genotyping Primers

Primer ID	Sequence (5'-3')	Probe	Allele
Ks_TWD1_For_FAM	<u>GAA GGT GAC CAA GTT CAT GCT</u> GCC TTG ACA TTG TTT TCA TCC TCA CT	FAM	7710S
Ks_TWD1_For_HEX	<u>GAA GGT CGG AGT CAA CGG ATT</u> GCC TTG ACA TTG TTT TCA TCC TCA CC	HEX	9425R
Ks_TWD1_Rev	GAA GTT CTG GTT ATA TGC TGT TAG GTC C	N/A	

*Probe-specific oligonucleotide sequences underlined

```

TAIR10_TWD1_cDNA
9425consensus_TWD1_cDNA_Locus_6992_Transcript_1/5_Confidence_0.583_Length_1532
7710consensus_TWD1_cDNA_Locus_6992_Transcript_1/5_Confidence_0.583_Length_1532

TAIR10_TWD1_cDNA
9425consensus_TWD1_cDNA_Locus_6992_Transcript_1/5_Confidence_0.583_Length_1532
7710consensus_TWD1_cDNA_Locus_6992_Transcript_1/5_Confidence_0.583_Length_1532

TAIR10_TWD1_cDNA
9425consensus_TWD1_cDNA_Locus_6992_Transcript_1/5_Confidence_0.583_Length_1532
7710consensus_TWD1_cDNA_Locus_6992_Transcript_1/5_Confidence_0.583_Length_1532

TAIR10_TWD1_cDNA
9425consensus_TWD1_cDNA_Locus_6992_Transcript_1/5_Confidence_0.583_Length_1532
7710consensus_TWD1_cDNA_Locus_6992_Transcript_1/5_Confidence_0.583_Length_1532

AACTAGCCGGTTAGCCATCGGGTGTG-----CTAGCATGAAGTCTGGTGAACGTGC 516
CCTTAAGCAGATCYTCTCTRGCTGCATCTGTTTGCCCTAGTTCGCTCTTGCTTTTCCTC 535
CCTTAAGCAGATCCTCTCTGGCTGCATCTGTTTGCCCTAGTTCGCTCTTGCTTTTCCTC 535
** * * * * * * * * * *

TTGTGCATGTTGGCTGGGAATTAGCTTATGG-GAAGAAGGAACITTTCTTTCCGAAT 575
GTCGTATAGTGCCTTGACATTTCTTCATCCTCACTAGGACAATGCTGCATT----- 589
GTCGTATAGTGCCTTGACATTTCTTCATCCTCACTAGGACAATGCTGCATT----- 589
* * * * * * * * * *

GTTCCACCTATGGCAGACTTGTATATGAGGTGGAACTTATTGGGTTTGATGAAACAA-- 633
-----GCATGATGGCATCCTCATAT-----TTCTTGAGCTTTATGTAACATGC 632
-----GCATGATGGCATCCTCATAT-----TTCTTGAGCTTTATGTAACATGC 632
* * * * * * * * * *

AGGAGGAAAAGCTCGCAGTGATGACTGT---AGAGGAAAGGATTGGTGC--AGCAGA 688
AGCAATGTTGAGATGGCAAGGATTCTTCACAGCCAGGCCATATCACGATACTCCCAA 692
AGCAATGTTGAGATGGCAAGGATTCTTCACAGCCAGGCCATATCACGATACTCCCAA 692
** * * * * * * * * * *

```

Figure 14 – TWD1 cDNA Alignment. Clustal Omega alignment of partial TWD1 cDNA sequences from 7710S 9425R, and *A.thaliana* (Col-0) shows the T572C substitution, which confers the S262G codon change (7710S->9425R).

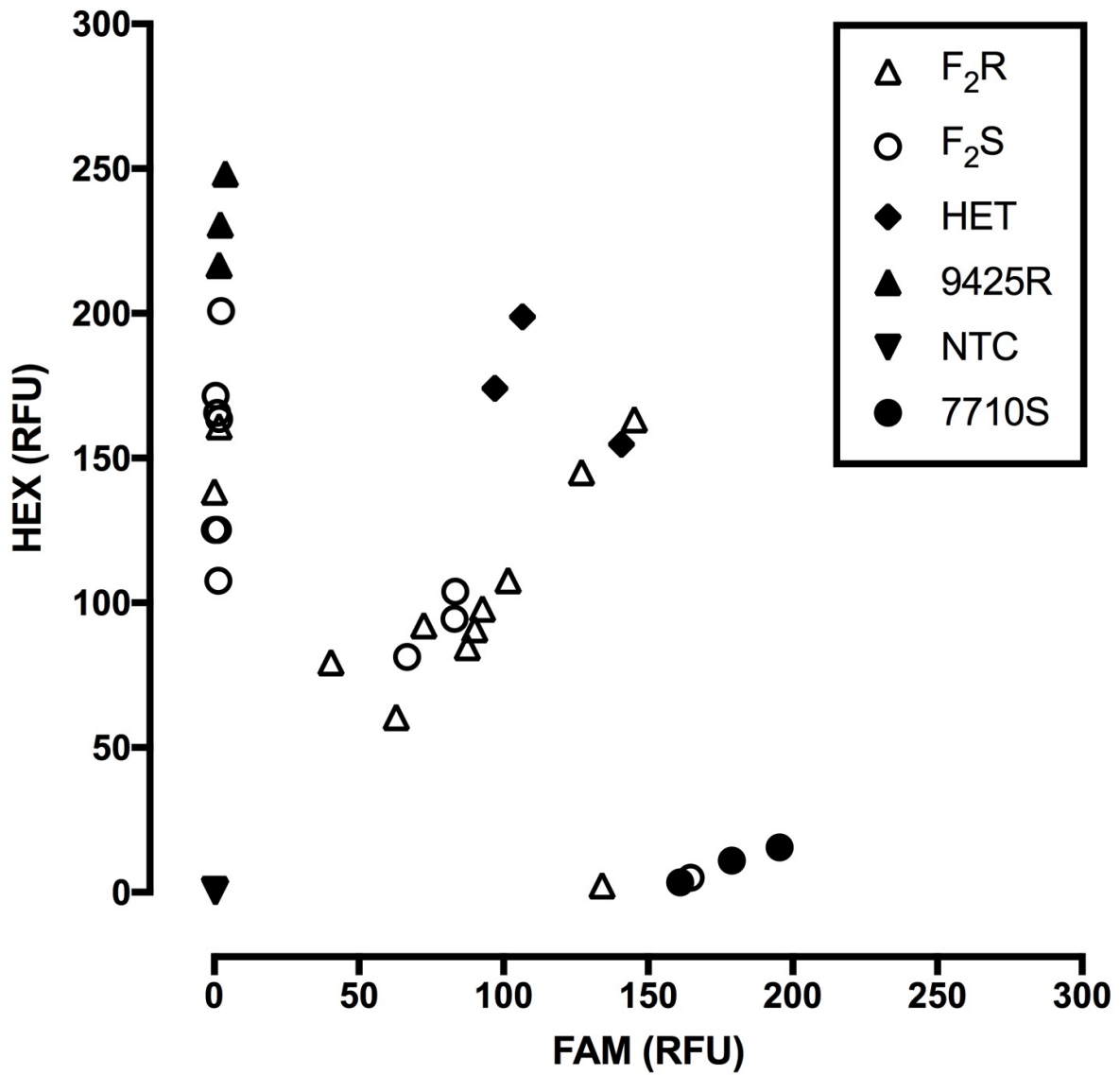


Figure 16 – TWD1 F₂ Genotyping. KASP assay for S262G mutation does not show co-segregation of 7710S and 9425R genotypes with their respective phenotypes in the F₂ population. RFU = relative fluorescence units.